A Study of Dark Matter Models at $\sqrt{s} = 13\,\text{TeV}$ pp Collisions for Mono-Lepton Searches.

von **Dennis Noll**

Bachelorarbeit in Physik.

vorgelegt der
Fakultät für Mathematik, Informatik und Naturwissenschaften
der RWTH Aachen

im
Juli 2015

angefertigt im
III. Physikalischen Institut A

bei

Prof. Dr. Thomas Hebbeker

Contents

1 Abstract **1**

2 Introduction **2**

3 Theory and Principles **3**
3.1 The Standard Model of Particle Physics . . . 3
3.2 A Dark Matter Model of Particle Physics . . . 4
3.3 Dark Matter Searches . . . 4
3.3.1 Direct Detection Experiments . . . 5
3.3.2 Indirect Detection Experiments . . . 5
3.3.3 Production at Colliders - EFT and Simplified Models . . . 5
3.4 Collider Search at the CMS System and Important Quantities . . . 6
3.5 DM Production at Colliders - Mono-X Channels . . . 8

4 The Model Setup **10**
4.1 Model Specific Parameters . . . 10
4.1.1 The Axialvector Model (AV) . . . 12
4.1.2 The Scalar Model (S) . . . 13
4.1.3 The Pseudoscalar Model (PS) . . . 13

5 The Analysis & Computing Setup **15**
5.1 The Event Generation & Selection . . . 15
5.1.1 Event Generation with Madgraph 5 . . . 15
5.1.2 Event Generation with the JHUGen . . . 15
5.2 Computing Setup and Technical Limitations . . . 16
5.2.1 Full Simulation with GEANT4 . . . 16
5.2.2 Mono-e Channel Cross Section . . . 17
5.2.3 Computation Simplification in MadGraph . . . 17
5.2.4 JHUGen Cross Section Scale . . . 17
5.2.5 The Boltdmdec . . . 18

6 Discussion of the Results **22**
6.1 Axialvector Model (AV) . . . 22
6.1.1 Shape Analysis in the AV Model . . . 22
6.1.2 Cross Section Analysis in the AV model . . . 30
6.1.2.1 Cross Section Analysis - $\mathbf{\Gamma^{min}_{med}}$ . . . 30
6.1.2.2 Cross Section Analysis - $\mathbf{\Gamma^{full}_{med}}$ . . . 31
6.1.2.3 Cross Section Analysis - $\mathbf{\Gamma^{Z}_{med}}$ . . . 32
6.2 Scalar Model (S) . . . 36
6.2.1 Shape Analysis in the S Model . . . 36
6.2.2 Cross Section Analysis in the S Model . . . 39
6.3 Pseudoscalar Model (PS) . . . 40
6.3.1 Shape Analysis in the PS Model . . . 40
6.3.2 Cross Section Analysis in the PS Model . . . 44
6.4 Model Comparison of the AV, S and PS Model . . . 45
6.5 The Background . . . 48

7 Summary of the Observations **49**

8 Future Prospects **50**

1 Abstract

A significance study considering new physical findings in proton proton collisions with leptons and missing transverse energy ($\not{E}_T$) in the final state is performed for a center of mass energy of 13 TeV.

The discovery of Dark Matter (DM) is one of the main tasks of the LHC analysis for 13 TeV and 14 TeV data. As well as other discoveries like large extra dimensions and quantum black holes DM has a signature which shows a large imbalance in transverse energy. An analysis of the DM production in CMS at generator level is performed. This analysis uses a simplified model where the DM particle is assumed to be a weakly interacting massive particle (WIMP) and is directly produced by a mediator particle (med). This DM particle is assumed to be a Dirac fermion.

The process is studied in different ways, in terms of cross sections (xsecs) and shape, concerning different coupling structures and strengths for the mediator particle coupling to Standard Model matter (in the following called matter) and DM. We will study three different mediator models. These models distinguish in the structure, how the mediator particle couples. These models are the axialvector (AV), scalar (S) and pseudoscalar (PS) model. Whithin these models, we will vary the coupling strenght.

Former analyses assumed that the coupling strengths DM↔med and matter↔med are equal in the DM generation process.

Such an analysis concerning different coupling structures and different coupling strengths for DM↔med and matter↔med has never been done before. It shall extend the assumptions about the coupling structure and strength in former papers, to 'fully map out the MSDM[1] landscape' [1]. Different mediator and DM masses are discussed in the background of this simplified model as well.

To connect the generator level processes with the experiment, full simulations with respect to the CMS system are done. Then the expected limits can be set into the parameter space of the simplified model.

This paper shows that the different couplings scale the cross section in dependence of the coupling strength but provide new analysis methods when concerning the difference in the shape of the signals for different coupling structures. It shows, that the difference in cross section and shape concerning different coupling structures are huge. We show that the AV model is the best model to study processes with a heavy mediator particle and the PS is the best model to study processes with relatively light mediators.

[1] MSDM stands for Minimal Simplified Dark Matter

2 Introduction

Since the beginning of mankind, physicists try to explain our world and its surroundings. They try to find the fundamental building bricks, our world is made of. In the ancient world, an atom was thought to be one of these bricks. The atom was named after the Greek word átomos that means undividable. It was common knowledged that it was one of the fundamental indivisible building bricks of our universe. It was only in the last century that these fundamentals were divided into even smaller parts. Scientists found that the atom consists of protons, neutrons and electrons. It took some more time to find that these protons and neutrons consists of quarks. Gauge bosons were discovered and a model was build, describing all the processes on this minor scale with tremendous precision: The Standard Model of Particle Physics (SM).

Even if the SM provides precise predictions concerning the subatomic processes, it does not explain every observation in the observable universe. Still there are hidden physics and open issues Beyond the SM (BSM), such as the theory of gravitation, the ratio of the electroweak and gravitational energy scales and the existence of Dark Matter (DM) to name a few. Some of those observations lead to new physics and challenge the existing principles and their validity limits.

The existence of DM and its gravitational influence on kinematical processes on the scale of galaxies has been demonstrated in astronomical measurements. Although the existence and the influence of DM are known, the subatomic nature of DM, the production and physical behavior on a subatomic scale are still not explained.

This vagueness about the particle nature of DM [2] calls for assumptions in the physical discussion of a DM particle, based on the DM observations in our universe. These assumptions include the nature of a possible DM particle, in detail the production, couplings and particle identity. Other observations conclude the DM particle to be weakly interacting, a Dirac fermion and possibly coupling to matter over a vector, axialvector, pseudoscalar or a scalar particle.

This bachelor thesis researches various models of DM generation. Those models are simplified models, where the DM is produced as a Dirac fermion from a decayed mediator particle recoiling against a W boson, with a mono lepton and missing transverse energy in the final state. Thus a Monte Carlo (MC) generator study of DM production at tree level and a full simulation in the CMS system are set up for a total center of mass energy of 13 TeV. A study at generator level shows the impact on various direct and indirect observables like the M_T shape and the total cross sections (xsecs).

3 Theory and Principles

3.1 The Standard Model of Particle Physics

The theory of the Standard Model (SM) of particle physics that was mostly finished in the 1970's describes processes at the subatomic scale with enormous precision. It lists all fundamental particles known so far as well as their interactions: electromagnetic, weak and strong. It consists of 6 different quark (3 uptype and 3 downtype) which couple via and to the gluons over a color charge and are electrically charged. And of 3 different leptons, 3 appendant neutrinos and additionally the five force transmitting bosons. Electroweak charged particles couple with the weak force via $W^{+/-}$ and Z bosons. The photon mediates as a particle of the electromagnetic force between electronically charged particles. Additionally there is the Higgs boson as a fifth type of boson.

Particle	interaction
γ Photon	electromagnetic
$W^{+/-}$/Z	electroweak/weak
8 gluons	strong

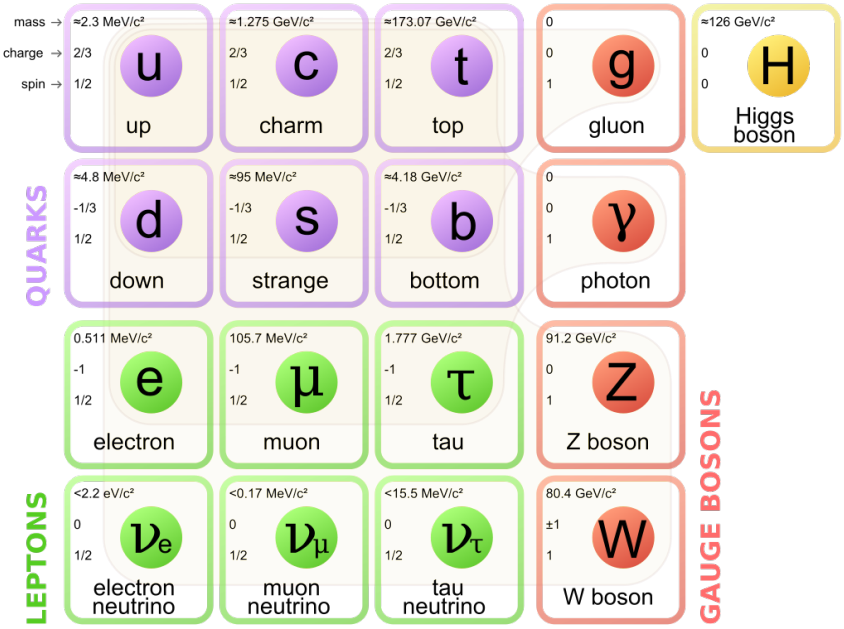

Figure 1: The Standard Model of particle physics [3]. It includes the fundamental particles and their interactions. The interactions between the bosons and the fermions are marked with the background colors. The Higgs boson couples to all particles with a mass.

To every fermion in the SM there exists an anti particle with opposite electromagnetic charge but same mass. The mathematical base of the SM is a Quantum Field Theory (QFT) where every particle is described by its appendant field. Although the Standard Model makes very precise predictions it cannot describe all the interactions and observations in our universe. For example, the SM as we know it does not incorporate the full theory of gravitation.

Additionally, the SM cannot describe the Dark Matter in our universe.

It needs a 'Beyond the Standard Model' (BSM) search to study DM processes.

3.2 A Dark Matter Model of Particle Physics

The existence of DM in our universe is shown by astrophysical measurements, such as the 'rotational speed of galaxies and gravitational lensing' [4]. Those prove that the density of matter with gravitational interaction in our galaxy is a lot bigger than the density of the matter (stars,clouds, etc.) we can observe. This leads to the conclusion that another unobservable type of matter exists in our galaxy.

Even if the existence of DM in our universe is established, the particle nature of DM is yet totally unclear. The main goal of the DM searches is to create a completed picture of the DM particle (χ) BSM.

The usual approach for DM search is to assume the DM particle to be a 'weakly interacting massive particle' (WIMP). This idea is justified by several observations on the DM in our universe:

> A hypothetical DM particle has to be stable, with a lifetime longer than the age of the universe, in terms of SM matter because one would have detected decay products otherwise[2].
>
> It has to be electrically and color neutral, this is what 'dark' means.
>
> And it has to be massive and weakly interacting ($\Omega_{\mathrm{CDM}}\cdot \mathrm{h} \propto 0.1$)[3], reasoned by cosmological measurements.

3.3 Dark Matter Searches

Basically there are three different strategies to search for DM. Those will be explained in this section:

- direct detection - where one aims to measure the recoil of a DM WIMP to a nucleus and the resulting energy emission
- indirect detection - DM could possibly annihilate and produce matter that one can actually measure
- production at colliders - produced DM would leave signals with $\not{E}_T$ in the detector

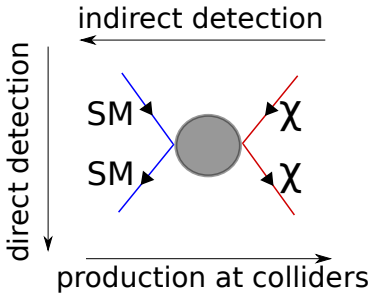

Figure 2: This schematic drawing shows the different channels of the different search strategies. The different searches focus on totally different channels. All of these channels incorporate an interaction of matter and DM.

[2] A hypothetical decay from a DM particle into an other DM particle would be theoretically possible. This decay would be equally invisible as the DM itself. Just a hypothetical decay from DM into SM matter can be excluded

[3] The λ_{CDM}-model is a model that describes the evolution of the universe with six parameters since the beginning of time. In this model Ω_{CDM} is one of the free parameters.

3.3.1 Direct Detection Experiments

Direct detection experiments try to measure the recoil of a DM particle, that hit a SM nucleus.The resulting energy emission is measured with different techniques [5].

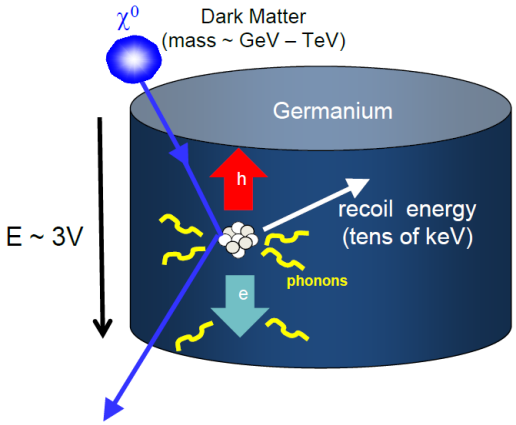

Figure 3: A schematic drawing of a direct DM detection [6] experiment. It shows the recoil of a DM particle and a matter nucleus in the detector.

To shield the experiment from cosmic rays and other backgrounds the detectors are located deep underground. A very high sensitivity is the main requirement for these detectors because a possible energy emission would be very low and even so deep underground ($1 - 2\,\mathrm{km}$) the background is very high. Because of the relative motion of Earth through the dark matter halo in our galaxy one expects an annual modulation of the dark matter signal [6].

3.3.2 Indirect Detection Experiments

Indirect detection experiments try to measure a possible annihilation from DM and a generation of matter such as gamma rays, charged leptons and neutrinos [7].

3.3.3 Production at Colliders - EFT and Simplified Models

This work focuses on a generator study for the production at colliders (last point in Fig. 2) where matter is supposed to annihilate in particle accelerators and produce DM in the final state. The decay of a so called mediator produces the DM. One example process for the production at colliders is shown for two different coupling models (to be explained in section 4.1) in Fig. 7 and Fig. 8 . More about the detection principles in the collider search is detailed in section 3.5.

The two different types of models for DM searches at colliders are Simplified Models or effective field theories (EFT). An EFT studies the effective process of the DM generation by assuming a very heavy mediator and very strong couplings. Just the final and the initial state are characteristic for a process. The hard process itself is done in a four way vertex, that only describes the process effectively. In the EFT approach, the signal of the process is determined by the structure of the interaction in the four way vertex and the mass of the DM particle only [8].

In contrast a simplified model assumes a hypothetical particle, a so called mediator (med) between matter and DM that is directly accessible in the simulation. This med cannot be resolved in an EFT search.

Simplified models have the advantage that they allow to study both the DM particle and the mediator, which is assumed to be a BSM particle as well, at the same time. It gives a better resolution for the full event kinematics and all process parameters can be dissolved in a

simplified model analysis. For a complete picture of a DM generation process it is essential to study the simplified model in order to scan the full process and to really understand the full kinematics of the event.

EFT and Simplified Model give comparable results at an interaction scale of $\approx 5000\,\text{GeV}$ [9] at the LHC for a center of mass energy of 13 TeV.

3.4 Collider Search at the CMS System and Important Quantities

The compact muon solenoid (CMS) [10] is a multi-purpose detector at the Large Hadron Collider (LHC), the biggest and most powerful particle accelerator in the world, located under Geneva at the European Organization for Nuclear Research (CERN). The CMS system is one of four general purpose particle detectors at the LHC, designed to measure subatomic particles. CMS is designed to measure multiple particles, their momentum, energy and their origin from proton proton (pp) collisions at the LHC.

The CMS detector is built of different detectors that are arranged around the LHC beampipe, see Fig. 4.

CMS has a barrel region and an endcap region and different detectors. Additionally a superconducting solenoid builds up a magnetic field of 3.8 T, to bend the particle tracks, essential to measure the momentum of the particles by their bending in the detector. The different detectors are located in tiers around the beam pipe and in the endcaps.

A schematic picture of CMS is shown in Fig. 4. From inside out it contains [11]:

- Silicon Trackers - consisting of the pixel and strip detector, here the first hits are registered and the particle traces are tracked. In this detector one can even see the first vertices from the Feynman graphs of the process.

- Electric Calorimeter (ECAL) - used to measure the energy of electrically interacting particles such as photons, electrons and positrons, particularly the E_T of electronically charged particles.

- Hadronic Calorimeter (HCAL) - a sampling calorimeter with absorber plates and scintillator plates, detecting hadrons.

- Muon Chambers - huge gaseous detectors covering the outer parts of the CMS system, just muons reach this part of the detector and can be detected accurately.

The hard scattering process of the subparticles of the two protons can be reconstructed using their detector outcomes. Thus a scattering process that takes place in the beam pipe can be identified by its final decay products.

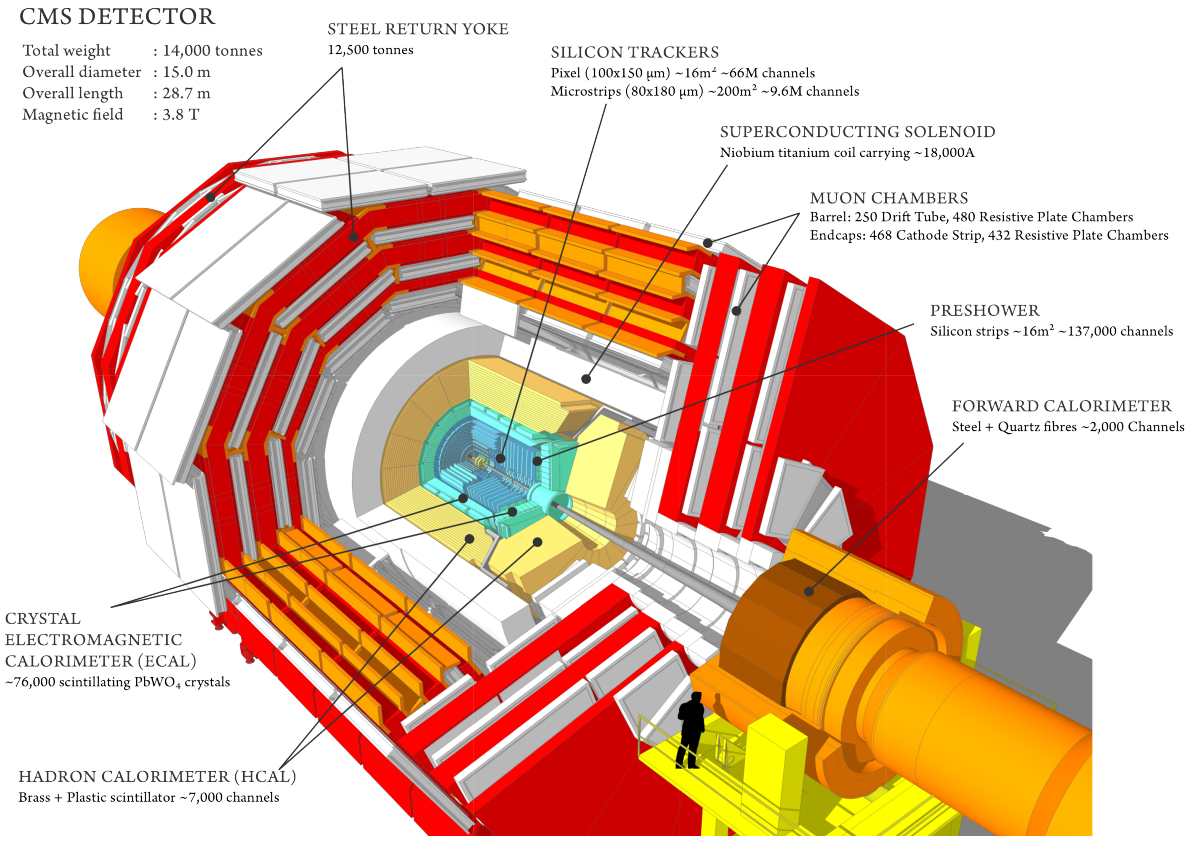

Figure 4: The CMS system at the LHC with its different detector elements [12].

To handle the geometry in the CMS detector, a new system of units has been established. The main quantities in this geometric system are *eta* and ϕ that will be explained below. The detector is build up cylindrical around the beam pipe. That is why it makes sense to take a cylindrical system of units. In the system of choice, ϕ is the azimutal angle. We expect all the distributions measured in the LHC to be ϕ-invariant, because all the elements (collider and detector) are constructed ϕ invariant as well. For a single event ϕ has an important role, especially in searches with $\not{E}_T$ as we will see in the next sections.

The second important quantity is η called the pseudorapidity, which is a measure for the polar angle, seen from the detector middle. It is defined by:

$$\eta = -\ln\left[\tan\left(\frac{\theta}{2}\right)\right]$$

with θ being the usual polar angle from sphere coordinates.

The two mentioned quantities are visible in Fig. 5 and Fig. 6. In Fig. 6 it is shown, that the positive η values are in a westerly direction

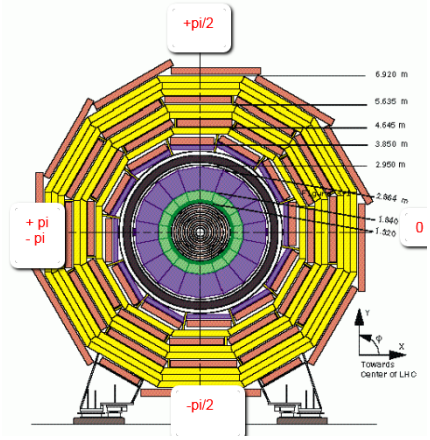

Figure 5: The different ϕ in the CMS system. The detector is shown in a transverse plane [12].

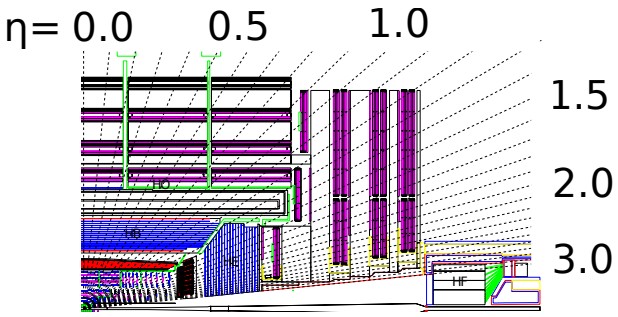

Figure 6: The different η in the CMS system. The detector is shown in a longitudinal plane [10].

Quantities that can be measured (direct- or indirectly) in the detector are the transverse energy (E_T), the missing transverse energy ($\not{E}_T$) or the transverse mass $\mathrm{M_T}$ for example. Whereas the transverse energy $\boldsymbol{E_T}$ is defined as a projection of the measured energy to the radial axis by:

$$E_T = \mathrm{E} \cdot \sin(\theta)$$

The missing transverse energy ($\boldsymbol{\not{E}_T}$) stands for all the particles that cannot be measured in the transverse plane, such as neutrinos or a possible DM particle. Because the transverse momentum and energy must be conserved perpendicular to the beam axis, the $\not{E}_T$ can be calculated back from the measured transverse energy E_T.

Usually we scan a distribution concerning the transverse mass $\mathbf{M_T}$. This transverse mass is defined as follows:

$$\mathrm{M_T} = \sqrt{2 \cdot E_T \not{E}_T \cdot (1 - \cos(\Delta\phi))}$$

with $\Delta\phi$ being the angle between E_T and $\not{E}_T$.

3.5 DM Production at Colliders - Mono-X Channels

This bachelor thesis discusses a DM particle that is produced in a single lepton + $\not{E}_T$ channel. In this particular channel, a mediator (med) produced in a proton proton collision decays into the DM, recoiling against a W that decays into a lepton and its neutrino, see Fig. 19.

The DM is assumed to be a WIMP, therefore, it leaves no energy or track in the detector. Due to the overall transverse energy before a collision being zero and the momentum conservation in every direction, the DM can be identified and detected via $\not{E}_T$. If one would search in a channel where just one generated mediator decayed to DM there would be just missing overall energy (which cannot be detected) and no signal would be detectable. Thus one is looking in channels where the quarks first radiate any particle that can actually be detected (eg. W or Z boson or jet). So it is possible to detect an imbalance in transverse energy when searching in a single event with DM production. This first radiated particle can be a gluon, γ or an other boson like W or Z e.g..

The main mono-X channels are:

- mono jet
- mono γ
- mono W (W$\rightarrow$ hadronic or W$\rightarrow$ lν)

- mono Z (Z→ hadronic or Z→ ll)

All these channels provide different features, advantages and disadvantages. The mono-jet and mono-γ searches have a huge background in the detector. The mono-jet channel has its high background from dijet processes (channels with two jets in the final state), in which one jet is not triggered the right way and a mono-jet event is registered for the analysis. The mono-γ background is due to a lot of channels with a mono-γ final state. These two channels have nevertheless high cross section, because of the big influence from strong interaction processes to the total cross sections in a collider at high energies The total inelastic cross section at the LHC for 8 TeV data was $\sigma_{\text{inel}} = 74.7 \pm 1.7\,\text{mb}$ [13]. The main contribution to this total inelastic cross section comes from strong interaction processes. This gives a hint, how high the background is distributed for the different search channels. The hadronic channels have a huge background.

The main difference between the channels with radiated W and Z bosons that decay leptonic, compared to the rest is, that in all other channel there is a very high background and no clear signals. In contrast to that, W bosons can decay into leptons and their neutrinos mainly behind a SM W background.

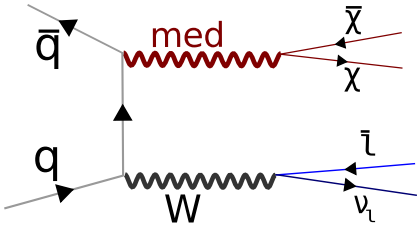

Figure 7: A Feynman graph of DM production in a simplified model for the mono-W channel. The mediator couples like an AV.

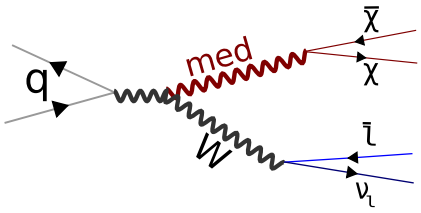

Figure 8: A Feynman graph of DM production in a simplified model for the mono-W channel. The mediator couples like a S or PS.

The decision to search in the W-channel provides several advantages: The radiated W decays into a lepton and its neutrino. The decay into one lepton provides a minimal background noise, compared to a possible presence of jets in different other channels, such as single jet & $\not{E}_T$ channels. This single lepton + $\not{E}_T$ channel provides a clear signal in the electromagnetic calorimeter or the muon chambers, and a possibly very large $\not{E}_T$ caused by the DM and the neutrino additionally [4]. Further on, in contrast to the mono-Z channel it provides a sensitivity to a difference in the DM couplings to up- and downtype quarks see Fig. 12 (characterised by ξ - introduced in 4.1).

For an impression how the process looks in the detector and to get an idea about the kinematics, the following figure shows the mono e + $\not{E}_T$ process:

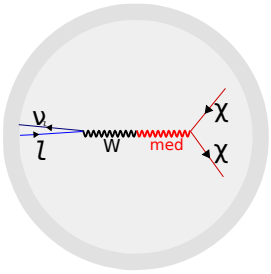

Figure 9: Schematic drawing of a mono-e + $\not{E}_T$ event in the detector. The W and the mediator recoil. No jets are present.

[4] Visible in the shape analysis of the AV

4 The Model Setup

4.1 Model Specific Parameters

Because we know little about DM and its physical properties several reasonable assumptions about the DM particle are made [14]. The DM particle is assumed to act like a Dirac fermion. This assumption is made in analogy to the known matter. That is why a discussion of the physics of the DM particle with respect to its parameters is possible. A simplified model where the mediator is specified is then characterized by four parameters:

- M_{med} - mass of the mediator
- M_{DM} - mass of the DM particle and antiparticle (χ and $\bar{\chi}$)
- $g_{q/W}$ - coupling strength between the mediator and a quark/W-Boson
- g_{DM} - coupling strength between the mediator and the DM

A zoom into the total process Feynman graph (see Fig. 7 and Fig. 8) shows where the four parameters are located in the process, see Fig. 10 and Fig. 11. These parameters are called 'model parameters' below.

Additionally to those model parameters, the mediator can couple differently - like an axialvector, vector, scalar or pseudoscalar, these coupling structures identify the below so called 'models'. To resolve a wide range of possible DM generation processes, the DM generation process is scanned for these models (see the theoretical background in section 4.1.1 (axialvector), section 4.1.2 (scalar) and section 4.1.3 (pseudoscalar)[5].

Model	Symbol
Axialvector	AV
Scalar	S
Pseudoscalar	PS

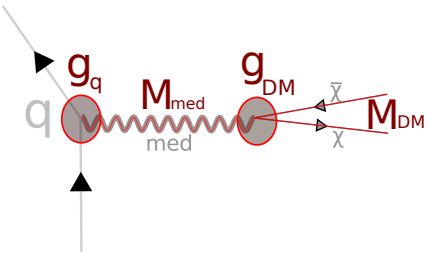

Figure 10: The four model parameters in the AV model. The coupling parameters $g_{q/W}$ contribute on the marked vertices.

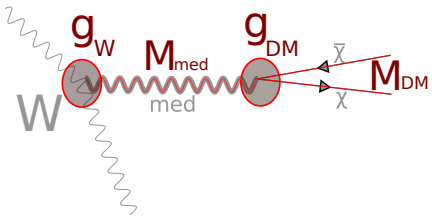

Figure 11: The four model parameters in the S/PS model. The coupling parameters $g_{q/W}$ contribute on the marked vertices.

Additionally the mediator has a width $\Gamma_{med}(M_{med}, M_{DM}, g_{q/W}, g_{DM})$, that contributes to the cross section and depends on the coupling structure as well as on the coupling strengths. This width influences the cross section of a process reciprocally. For a s-channel process this would be proportional to:

$$\sigma \propto \frac{g_{q/W}^2 \cdot g_{DM}^2 \cdot s}{(s - M_{med}{}^2)^2 + s\Gamma_{med}^2} \tag{1}$$

[5]The 'vector only' case is not discussed. Former analyses show that AV and 'vector only' processes do not differ substantially.

Here s is the center-of-mass energy of the parton system. Equation 1 shows that $\sigma \propto 1/\Gamma$, hence small widths are preferred to get maximum cross sections and due to this maximum sensitivities.

usual approach: smaller widths ⇒ larger cross sections ⇒ better sensitivities

Till now the simplified model analysis focused on the same coupling strength on the side of DM and matter ($g_q = g_{DM}$).

The two coupling strengths contribute to the process in two ways. First they change the cross section of a process by variation of the mediator width (see equation 1). Second they change the kinematics of the process.

In the study of the AV model, three different width approaches will be discussed and the results in terms of different resulting cross sections will be pointed out in the AV case.

A scan of the mediator and DM masses has already been done in an EFT model and is fairly studied [9][6].

To fulfill the requirements of perturbation theory, the mediator width has to be smaller than a third of its mass:

$$\Gamma_{med} \overset{!}{\leq} \frac{M_{med}}{3} \tag{2}$$

This creates a theoretical upper bound of the mediator width. However this value is just a guideline, corresponding to the point where the next-to-leading-order (NLO) term in the perturbation theory is equal to the leading-order (LO) term ($\sigma_{NLO}/\sigma_{LO} \approx \mathcal{O}(1)$). Above this constrain, the generated events are not physically motivated anymore in the LO. The cross section is dominated by higher order effects.

One additional parameter is needed for a channel including a W boson. For a channel with a W, it is possible to make a difference between the DM particle coupling to up- or down-type quarks. The initial and final states of these processes (see Fig. 12) are equal. Therefore some kind of interference occurs between these processes. A new parameter (ξ) is introduced as an interference parameter (see [15]). This parameter parameterizes processes with constructive and destructive interference between up- and down-type type quark processes and is often chosen to be $\xi = \pm 1,0$.

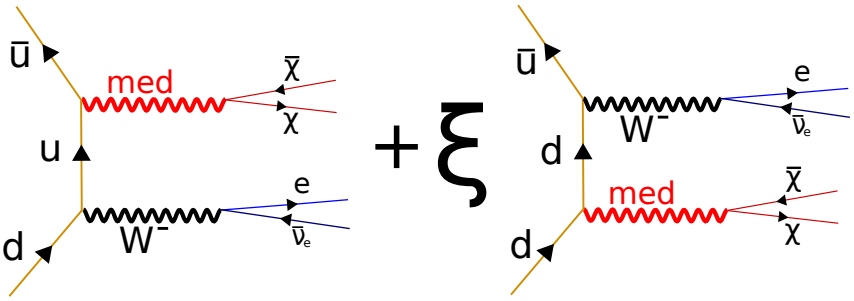

Figure 12: The interference parameter ξ, between up- and down-type quark processes. This parameter determines the interference of the processes where the mediator couples to up- or down-type quarks.

Former analyses [14] [15] show that the differences for different ξ in terms of the cross sections are huge (about one order of magnitude). The case $\xi = -1$ gives the maximum sensitivities and the largest cross sections- it is called the constructive interference. In a theoretical paper [16], it was recently shown for an EFT approach, that $\xi = -1$ is not physically reasonable (without

[6]The approach in the mentioned paper is to analyse the cross sections for a constructive interference case only and mostly compare the interference cases in respect to their M_T shape.

extensions to the model) because the raise in cross sections comes from longitudinally polarized W bosons as a result of breaking ward identity.

If this argumentation holds for a simplified model as well on the theoretical side is yet unclear.

However this effect appears in all channels where DM and a W boson are produced in pp collisions. If the cross sections of the DM production can be measured in a collider, a comparison to the different interference cases with comparison to the measured cross sections discloses a sensitivity to this parameter ξ and allows us to study the nature of DM in a new way.

To keep a fair comparison with former results and EFT searches, the following analysis is done for the conservative choice of the $\xi = +1$ case only.

It has not been discussed yet, but is also possible, that there is not only one DM particle but a real structure. That would leave us with a vast range of different DM particles and thus a vast range of different analyses and simulations. Just assuming to search for one DM particle in the beginning is a simplification of the search. This simplification is reasonable because maybe, as it was the case in former SM discoveries, one decay channel and one mediator might play a dominant role [8].

4.1.1 The Axialvector Model (AV)

The first and best studied model till now has an assumed axial-/vector mediator.

During the writing of this thesis a forum of experimental physicist from CMS and Atlas as well as theoretical physicists was established. This forum agreed on several common parameters for the simplified model, see [8].

One of the recommendations is to search for pure vector (V) or axialvector (AV) couplings.

Mixed couplings to DM and matter could be possible as well but to minimize the computation effort, just the recommended case is discussed here.

We showed in former analyses, that just a negligible small difference (for all observables) exists between the AV and the V coupling structure in the simplified model [9] [14]. The physical difference between these coupling structures is that the AV coupling shows an extra sensitivity to the spin. This work focuses on the AV case only[7]. The following Lagrangian incorporates the AV coupling of the mediator to the different quarks ($\sum_q$) and the DM particle.

$$\mathcal{L}_{\text{axial}} = \sum_{q} g_q Z'_\mu \bar{q} \gamma^\mu \gamma^5 q - g_{DM} Z'_\mu \bar{\chi} \gamma^\mu \gamma^5 \chi \tag{3}$$

Because the couplings affect the cross section by varying the mediator width (see equation 1) it makes sense to discuss the mediator width especially. Till now, the standard approach was to take a narrow mediator width of $\Gamma_{\text{med}} = M_{\text{med}}/8\pi$ and a maximal mediator width of $\Gamma_{\text{med}} = M_{\text{med}}/3$ to have outer bounds for an analysis [14].

By a paper about 'Dark Matter Searches at Colliders and Direct Detection Experiments' [17] dependencies between the couplings and the mediator width are summarized. The formulas for a heavy fermion width were taken from [17]. These formulas can be used to calculate the partial mediator widths:

$$\Gamma(\text{med} \to \overline{\chi}\chi)_{\text{axial}} = \frac{g_\chi^2 M_{\text{med}}}{12\pi} \left(1 - \frac{4m_\chi^2}{M_{\text{med}}^2}\right)^{3/2} \tag{4}$$

$$\Gamma(\text{med} \to \overline{q}q)_{\text{axial}} = \frac{n_c g_q^2 M_{\text{med}}}{12\pi} \left(1 - \frac{4m_q^2}{M_{\text{med}}^2}\right)^{3/2} \tag{5}$$

where n_c is the number of colors from a particular quark. Significant is, that for $g_q = g_{DM}$, the only difference for the mediator width contributed by a single particle (matter or DM) comes

[7] The AV case has been chosen because, in the generator search superior limits can be set compared to direct detection experiments. This is not the case for a 'vector only' coupling mediator, where the direct detection is a real competition to this analysis.

from the mass term, that appears like a mass correction term in first order. However the number of quarks is not determined by [17] and a free parameter in this model.

The total mediator width is given with:

$$\Gamma_{\text{med}}^{\text{total}} = \Gamma(\text{med} \rightarrow \overline{\chi}\chi)_{\text{axial}} + \sum_{\text{q}} \Gamma(\text{med} \rightarrow \overline{\text{q}}\text{q})_{\text{axial}} \tag{6}$$

The width models that are introduced below will be discussed in the AV model. The minimal number of SM quarks coupling to the mediator is one, because it has to be generated from matter first. This approach is called the 'min width approach' ($\mathbf{\Gamma_{med} = \Gamma_{med}^{min}}$). It is assumed, that the mediator couples to just one light quark (with negligible small mass $\rightarrow m_q = 0$) of one color. This coupling structure is not motivated in a physical reason but gives a lowest bound for the mediator width, which results in the largest cross section. In this case, if $g_q = g_{DM} = 1$, the mediator has the same width as in the 'narrow-width approach' ($M_{med}/8\pi$) but is even lower for $g < 1$. A coupling dependent mediator width for different couplings seems better motivated at all.

The naive approach would leave the mediator coupling to all quarks, with all colors. We call this the 'full width approach'($\mathbf{\Gamma_{med} = \Gamma_{med}^{full}}$). It generates the largest widths, is physically best justified[8] but leaves us with the smallest cross sections resulting in the worst sensitivities. The results will show that this case provides the worst exclusion limits in the case of a discovery due to the low cross sections.

Additionally to the two cases, motivated through formula 4 and 5, we discuss a model, where the mediator couples via an isospin-motivated coupling structure, where the DM has an isospin, and the mediator is SM Z like ($\mathbf{\Gamma_{med} = \Gamma_{med}^{Z}}$). This leaves us with a mediator width of:

$$\Gamma_{\text{med}}^{\text{Z}}(\text{med} \rightarrow \bar{\text{f}}\text{f}) = \sum_{\text{f}} \frac{N_c g_{\text{f}}^2 M_{\text{med}}}{24\pi} [(T_{3_{\text{f}}} - Q_{\text{f}} \sin\theta_w)^2 + (Q_{\text{f}} \sin\theta_w)^2] \tag{7}$$

Where the parameters are chosen to:

f	Q_{f}	$T_{3_{\text{f}}}$
u / c / t	+2/3	+1/2
d / s / b	-1/3	-1/2
DM	0	± 1/2

The electric charge of the DM particle is set to zero to validate the 'darkness' of the particle (as described in section 3.5).

4.1.2 The Scalar Model (S)

In the scalar model, the mediator is assumed to act like a scalar particle. This scalar field is invariant under Lorentz transformations [18]. The following Lagrangian describes the scalar particle:

$$\mathcal{L}_{\text{S}} = a\phi\bar{\psi}\psi \tag{8}$$

Until now the only known elementary scalar particle is the Higgs boson.

4.1.3 The Pseudoscalar Model (PS)

In addition to a scalar particle (see section 4.1.2) the mediator could also be pseudoscalar like. A pseudoscalar physical quantity flips sign under a parity transformation [18]. No pseudoscalar elementary particles have been discovered yet. Some mesons like the π^0 show a pseudoscalar

[8] This case is 'physically best justified' in the view, that no new quantum numbers have to be added to the model to justify the exclusive coupling to certain quarks.

coupling. The pseudoscalar coupling is very similar to the scalar coupling, but provides an extra spin sensitivity, that is expressed in the γ_5 term in the Lagrangian:

$$\mathcal{L}_{\mathrm{PS}} = b\phi\bar{\psi}\gamma_5\psi \tag{9}$$

Due to the recent discovery of the Higgs boson, the extension of the simplified model analysis also incorporates a pseudoscalar particle mediating between matter and DM.

5 The Analysis & Computing Setup

The event generation is performed at generator level with LO matrix element Monte Carlo (MC) event generators. Two different MC generators will be used. The Simulations of the axialvector (AV) coupling processes will be done with MadGraph 5 - v2.2.3 (MG) and the scalar (S) and pseudoscalar (PS) cases are treated by the JHU Generator - v5.2.5 (JHUGen).

Table 5.2.5 gives an overview of the different models and parameters.

5.1 The Event Generation & Selection

The center of mass energy in both generators is set to $\sqrt{s} = 13\,\text{TeV}$. The discussed events are characterized by a lepton with very high p_T in the final state allowing themselves to be measured and a high $\not{E}_T$ caused by the DM particles and the neutrino.

5.1.1 Event Generation with Madgraph 5

MG is one of the standard MC generators for SM and BSM physics at the LHC. This tool provides a wide range of possibilities to adjust the simulations for the needed processes and is documented well in the terms of usage.

In the event generation, a cut is set to a lepton $p_T^{lep} > 10\,\text{GeV}$. Additionally a p_T cut is set to possibly occurring jets to $p_T^{jet} > 20\,\text{GeV}$ to assure a correct description of the hard parton process and filter jets that occur aside the hard process. The AV events in MG5 are generated for the cross section analysis for the parameter sets at table 3.

First the mediator width is Γ_{med}^{min}. The parameters for the cross section analysis are chosen to cover a large parameter space. We want to look at differing different coupling strength g_q and g_{DM} (ranging from 0.1 to 2.0) for a variation of M_{med} (first tabular in table 3) and M_{DM} (second tabular in table 3). At last, a connection for the two different couplings g_q and g_{DM} should be found (third tabular in table 3).

The event generation for the cross section studies, is done with 200 events each. Generating so few events saves computation time and just raises the uncertainty of the cross section by a negligible small amount. For the shape studies, a generation with more events is needed to produce a convincing shape. Runs with 200000 events are produced for the parameter sets at table 4.

We also want to study the two other width models (Γ_{med}^{full} and Γ_{med}^{Z}). Computing the same parameter sets would take to much computation time. Because of this, they are discussed with a set of $M_{DM} = 500\,\text{GeV}$;$M_{med} = 1750\,\text{GeV}$;$g_q = 0.1, 0.2, 0.3, ..., 1.9, 2.0$;$g_q = 0.1, 0.2, 0.3, ..., 1.9, 2.0$ only.

5.1.2 Event Generation with the JHUGen

The JHUGen is a quite new tool for MC generation at generator level. Yet it is still being improved and obtained different new features.

The JHUGen enables us to scan the simplified model of DM generation with S and PS couplings.

This generator uses no cut on the leptons, but provides the possibility to set a cut on the jet p_T. Nevertheless, no radiated jets were used in the event generation with the JHUGen.

The runs are generated with 200000 events each for cross section and shape analysis. For S and PS, the simulation parameter set is given in table 5. We tried to get a full scan of the S and PS model in table 5 for the two varying simplified model parameters (M_{med} and g_W). Difficulties in the computation limit the parameter space. This will be explained is section 5.2.4 and section 5.2.5.

5.2 Computing Setup and Technical Limitations

5.2.1 Full Simulation with GEANT4

To build a link between simulated data to actual LHC data in further analyses, expected limits are prepared with a full simulation of the process with GEANT4 [19] in the CMS system. This is done for different integrated luminosities[9] (L_{int}) of 1, 30, 300 and 3000 inverse fb (fb^{-1}). The luminosities are a measure of the data collected by the CMS experiment, or put out by the LHC.

In simple words, the approach to produce such a limit is to take the MC generated distributions with (signal + background) and without (background) the expected signal. By comparing these two distributions, it shows how many events could have been observed above the background estimation if the signal was where we expected it to be.

Whereas 1 fb^{-1} is a low luminosity, 30fb^{-1} is the luminosity provided by the 7 TeV and 8 TeV in run 1, a luminosity of 300fb^{-1} will be reached after the 13 TeV and 14 TeV runs (run 2) and 3000 fb^{-1} is a very high luminosity and will be reached after the so called 'high lumi' [20] (run 3).

These expected limits deliver a comparison, how well we could observe a signal and at which luminosity (at which amount of data) we could possibly make a discovery.

Because we talk about measuring data at this point, a comparison is needed how well a lepton is reconstructable into a signal that can be processed electronically in the CMS system. A measure for this is the efficiency. This efficiency is defined in the following without (ϵ) and with ($\epsilon_\eta^{\text{cut}}$) a cut on the background data:

$$\epsilon = \text{N}_{\text{Events}}^{\text{reconstructed}}/\text{N}_{\text{Events}} \qquad \epsilon_\eta^{\text{cut}} = \text{N}_{\text{Events}}^{\text{reconstructed}}/\text{N}_{\text{Events}}(\mid \eta \mid < 2.3) \tag{10}$$

where $\text{N}_{\text{Events}}^{\text{reconstructed}}$ is the number of the in the analysis reconstructed events and N_{Events} is the number of overall events in the detector. The number of overall events (N_{Events}) is calculated in a MC simulation. The following reconstruction efficiencies are given for electrons and muons in the detector:

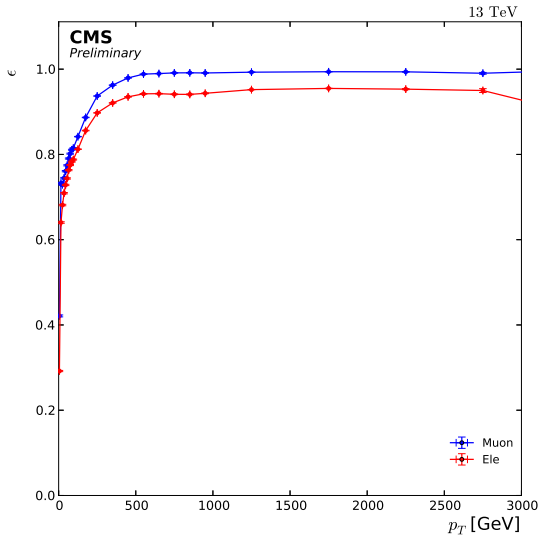

Figure 13: The reconstruction efficiencies ϵ for electrons muons in the CMS system, dependent on the lepton p_T.

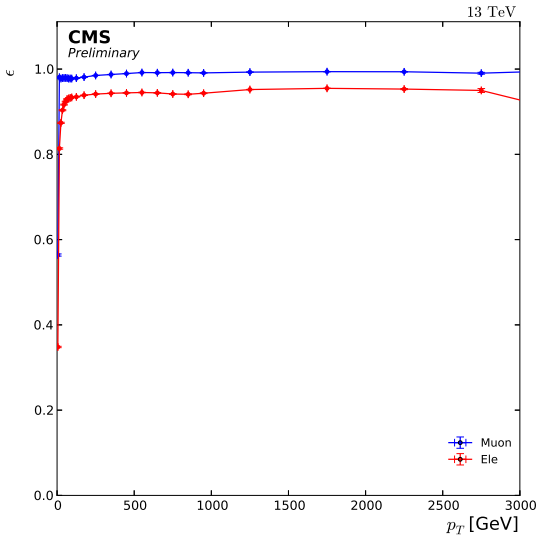

Figure 14: The reconstruction efficiencies $\epsilon_\eta^{\text{cut}}$ for electrons and muons in the CMS system, dependent on the lepton p_T. The generated particles have an $\mid \eta \mid < 2.3$ cut.

[9] In the following the integrated luminosity, which is a measure for number of detected events and thus a measure the collected data will be just called 'luminosity'.

The left graph shows the efficiency from MC data with every geometry, in the right graph, an $|\eta| < 2.3$ cut at generator level is applied.

The calculated limits vary with the shape (to see in section 6.1.1, 6.3.1 and 6.2.1) and thus with the mediator mass only, as we will see in the shape analysis. These limits can further be drawn into cross section plots for the parameter space.

In a data analysis in possible following papers to this model, there will be the standard cuts on single-lepton + $\not{E}_T$ from [14]. A $\Delta\phi(\text{lepton},\not{E}_T) > 2.4$ cut and a $0.4 < p_T^{lep}/\not{E}_T < 1.5$ cut on the lepton p_T to assure a back-to-back production between matter and $\not{E}_T$.

The expected limits are set at a 95% confidence level (CL) - what corresponds to roughly 2σ in a standard Gaussian distribution, with σ being the standard deviation.

5.2.2 Mono-e Channel Cross Section

Because we analyse a single lep + $\not{E}_T$ channel for one particular lepton (in this case the electron - mono-e channel), the cross sections are scaled form the 'all leptons' to the 'just electron' cross sections with the branching ratio (BR(W$\longrightarrow$eν_e)). Then the single electron and $\not{E}_T$ cross section is given by $\text{BR}(\text{W} \rightarrow \text{e}\nu_\text{e}) \cdot \sigma_{\text{all-leptons}}$. An other option is to just generate processes with a single electron and $\not{E}_T$ in the final state.

The 'scaling' option is chosen for simulations with the JHUGen, the second option is chosen for the simulations with MadGraph. The reason therefore is that in MadGraph one can precisely define the decay product of the W in a subprocess, with respect to all process participating particles, whereas in the JHUGen just a single leptonic decay (W$\longrightarrow$lν_l) can be defined.

5.2.3 Computation Simplification in MadGraph

One additional computation simplification is done in MadGraph, in the cross section analysis of the **AV** processes. The generation is done with light quarks (u and d) and gluons in the initial and final state to reduce the number of contributing Feynman graphs. This reduces the cross section by a constant factor. This way, the 'real' cross section (with all quarks, as in reality) can be calculated from the results with this factor. This simplification reduces the computation time by a factor of 20.

5.2.4 JHUGen Cross Section Scale

Initially the cross sections produced in the event generation with the JHUGen are relative cross sections. Phil Harris (et al.) [21] developed a tool to scale the relative cross sections back to absolute cross sections with the help of literature values.

Fig. 16, Fig. 17 and Fig. 18 show the scaling literature values that are given in the new patches provided in the JHUGen extension. The functions to scale the cross section back are called scaleup(*scale*), WH(M_med) and BRbb(M_med). The function scaleup(*scale*) scales the relative cross section back to the absolute ones. WH(M_med) is a correction dependent on the mediator and W mass. BRbb(M_med) is a correction on the $BR()$ to fermions assuming scalar decays to bosons. This function corrects the branching ratios of the W. Because the mediator couples to the W boson, the branching ratio from all other particles coupling to the W boson changes.

The scaling then works with the following function:

$$\sigma^{\text{scaled}} = \sigma^{\text{unscaled}} \cdot \text{WH}(\text{M}_\text{med}) \cdot \text{scaleup}(scale) \cdot var_{corr}$$

$$\text{with} \qquad scale = \text{M}_\text{med} + 80\,\text{GeV} + 15\,\text{GeV} \quad \text{and} \quad var_{corr} = \text{BRbb}(\text{M}_\text{med}) \cdot \frac{246^2}{4.8^2}$$

In this function the value *scale* is made of the W boson mass and an addition of extra energy based on matching the cross sections.

Just a small parameter space for M_{med} is prepared in this extension. For M_{med} values of $M_{med} > 1000\,\text{MeV}$ the scaling functions WH(M_{med}) and BRbb(M_{med}) (Fig. 17 and Fig. 18) are no more saved to the data and are extrapolated for the scale. This extrapolating function is a ROOT [22] inner tool and does not provide proper outcomes in this frame. Because of this the JHUGen samples can only be calculated for small mediator masses (see table 5).

5.2.5 The Boltdmdec

The JHUGen is meant to be a tool for a **S** or **PS** particle in the final state and does not include a decay into DM. Thus it is used as a tool for the mediator production and analysis only. Due to this the final state DM particles are not written into the LHE file.

Additional to the JHUGen, Chiaran Williams provides a tool called boltdmdec, to further decay the med to two DM paricles. This tool adds the two DM particles to the old LHE file as shown in the following chart:

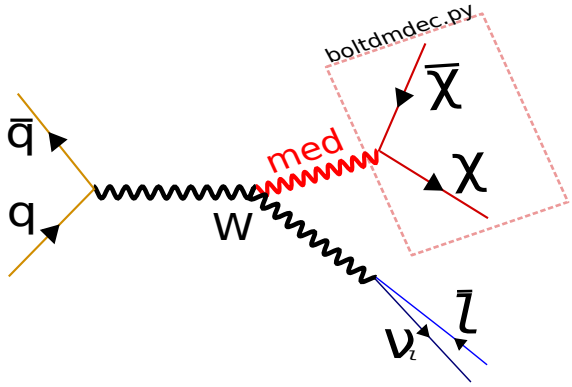

Figure 15: JHUGen - mediator to DM generation by boltdmdec

The boltdmdec merges the DM particle into the LHE file but does not change the cross sections of the process.

This can be corrected afterwards by assuming a total branching ratio ($BR(\text{med} \rightarrow \text{DM}) = 1$) from the mediator into the DM particles.

Because of this, the event cross section stays the same for all DM particles.

Due to this the cross sections can not be studied for different DM particles (see table 5) if we use the output of the JHUGen only. Additional calculations for the branching ratio med↔DM (BR(med→DM)) are possible but not executed within this thesis. We analyse a process with a mediator in the final state (in Fig. 15 the part of the process without the dotted box).

The shape analysis is possible for different DM particles because the boltdmdec takes care of the different DM particles in the simulation[10].

[10]The boltdmdec is very fragile when it comes to difficult processes in terms of high mediator masses and rends a phase space error. This error leads to errors in the shape calculation. This problem could not have been fixed in the simulations yet and cuts the possible mediator masses for the process generation.

Tabular 5.2.5 shows a summary of all models, parameters and the appendant studies.

Model	Axialvector			Scalar	Pseudoscalar
Symbol	AV			S	PS
Parameters	M_{med} M_{DM} g_q g_{DM}			M_{med} M_{DM} g_W g_{DM}	M_{med} M_{DM} g_W g_{DM}
Width[11]	Γ^{min}_{med}	Γ^{full}_{med}	Γ^{Z}_{med}	Γ^{nar}_{med}	Γ^{nar}_{med}
Shape	M_T $\eta^{lep/jet}$ $\phi^{lep/jet}$ $\Delta\phi$(W,med) $\Delta\phi$(W,ν)	-	-	M_T η^{lep} ϕ^{lep} $\Delta\phi$(W,med)	M_T η^{lep} ϕ^{lep} $\Delta\phi$(W,med)
Cross Section	M_{med} | g_q M_{med} | g_{DM} M_{DM} | g_q M_{DM} | g_{DM} g_q | g_{DM}	g_q | g_{DM}	g_q | g_{DM}	M_{med} | g_W	M_{med} | g_W

Table 1: This tabular shows a summary of all three models (AV/S/PS), their parameters and the appendant studies (shape and cross section). The width approaches are explained in section 4.1. The shape is studied for a variation of the listed parameters. The cross section studies are always done two dimensional (X|Y).

$M_{med} = 1750\text{GeV}; M_{DM} = 500\text{GeV}$

Parameters g_q/g_{DM}	ratio (%)
1/1	94,0
1/0.2	93,6
0.5/1	92,8
0.5/0.2	95,6
0.2/1	94,4
	$= 94,0 \pm 1,0$

Table 2: A variety of different simplificated runs. The cross section is just scaled within the computing simplification. The uncertainty which is caused by this procedure is negligible. The ratio is defined by ratio= $\sigma_{new}/\sigma_{old}$. Whereas σ_{old} is the cross section including all types of quarks, muons and electrons and σ_{new} is the cross section including just light quarks and electrons. The uncertainty is the standard deviation of the values. This uncertainty is an estimate of the real uncertainty, this process causes.

[11] The different widths are discussed in the theory section. $\Gamma^{nar}_{med} = M_{med}/8\pi$

In the following the different parameter sets for the computation are shown. The diagonal values are always constants. The parameters in the tabular are being varied. For each value on the left side, all values on the right side are varied and the other way around. This way, tabulars with two columns are two dimensional arrays in the parameter space.
Why the parameters are chosen this way is explained in section 5.1.1 and section 5.1.2.

$M_{DM} = \text{const.} = 500\,\text{GeV}$, $g_{DM}/g_q = \text{const.} = 1.0$

M_{med}[GeV]	g_q/g_{DM}
1001	0.1
1150	0.2
1300	0.3
1450	0.4
1600	...
1750	1.8
1900	1.9
2050	2.0

$M_{med} = 1750\,\text{GeV}$, $g_{DM}/g_q = 1.0$

M_{DM}[GeV]	g_q/g_{DM}
1	0.1
100	0.2
200	0.3
300	0.4
...	...
600	1.8
700	1.9
800	2.0

$M_{med} = 1750\,\text{GeV}$, $M_{DM} = 500\,\text{GeV}$

g_q	g_{DM}
0.1	0.1
0.2	0.2
0.3	0.3
0.4	0.4
...	...
1.8	1.8
1.9	1.9
2.0	2.0

Table 3: Parameter sets for the cross section studies in the **AV** model.

$M_{med} = 1750\,\text{GeV}$, $M_{DM} = 500\,\text{GeV}$

g_q	g_{DM}
0.1	0.1
0.2	0.2
0.3	0.3
0.4	0.4
...	...
1.8	1.8
1.9	1.9
2.0	2.0

$M_{DM} = 500\,\text{GeV}$, $g_q = g_{DM} = 1.0$

M_{med}[GeV]
1001
1300
1600
1750
1600
1750
2050

Table 4: Parameter sets for the shape studies in the **AV** model.

$M_{DM} = 10\,\text{GeV}$, $g_{DM} = 1$

M_{med}[GeV]	g_W
21	0.1
50	0.2
70	...
100	0.9
150	1.0
200	1.3
225	1.5
250	1.7
300	1.9
400	2.0

Table 5: Parameter sets for cross section and shape studies in the **S** and **PS** model.

The following functions are implemented in the used JHUGen patch. The functions are used to scale the cross section back. The cross sections produced by the JHUGen are scaled to arbritrary values. The scaling works with the following function:

$$\sigma^{\text{scaled}} = \sigma^{\text{unscaled}} \cdot \text{WH}(\text{M}_{\text{med}}) \cdot \text{scaleup}(scale) \cdot var_{corr}$$

$$\text{with} \qquad scale = \text{M}_{\text{med}} + 80\,\text{GeV} + 15\,\text{GeV} \quad \text{and} \quad var_{corr} = \text{BRbb}(\text{M}_{\text{med}}) \cdot \frac{246^2}{4.8^2}$$

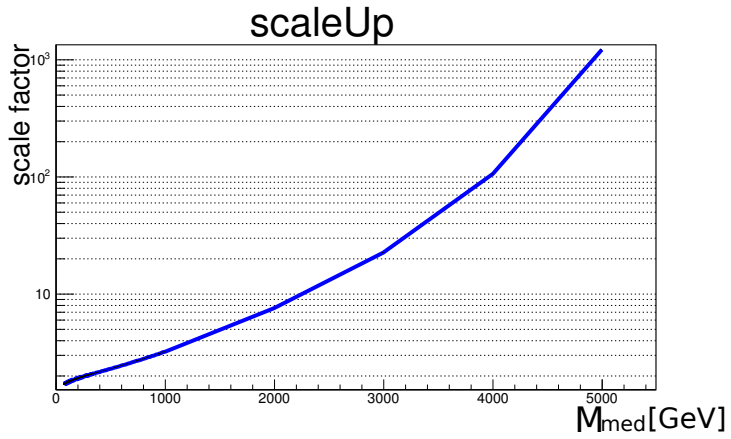

Figure 16: The Scaleup() function provided in the JHUGen extension.

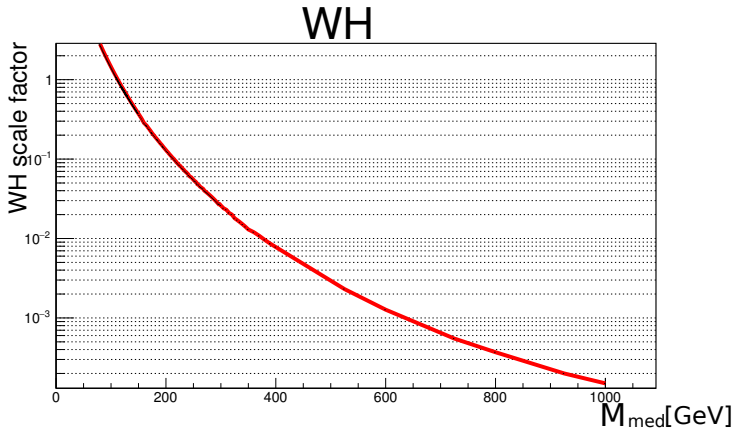

Figure 17: The WH() scale function provided in the JHUGen extension.

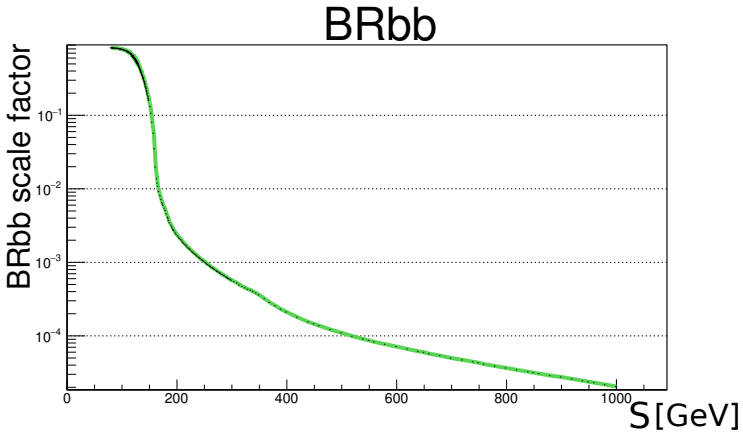

Figure 18: The BRbb() scale function provided in the JHUGen extension.

6 Discussion of the Results

The results of the simulations of the DM generation process will be discussed. First we discuss the three single models (AV - section 6.1, S - section 6.2, PS - section 6.3) which will then be compared to each other in section 6.4. We will first discuss the shapes (M_T,η,ϕ,..) for different parameters and then the event cross sections for different parameters[12]. These two different studies are performed for each model separately.

6.1 Axialvector Model (AV)

The first model to be discussed is the AV model starting with a shape analysis for different parameters and observables. We will see the influence of different model parameters to the shape. We will discuss that the 'main' shape (M_T) is changed for different mediator masses (M_{med}) and stays the same for different coupling strength (g_q/g_{DM}).

After analysing the shape, we will study the total event cross sections of the particular processes. Scanning the cross sections against the four model parameters gives a good impression of their impact on the process. To analyse the mediator width (Γ_{med}) extensively, we discuss three different width approaches ($\Gamma_{med} = \Gamma^{full}_{med}/\Gamma^{min}_{med}/\Gamma^{Z}_{med}$) in the cross section analysis.

6.1.1 Shape Analysis in the AV Model

In the shape analyses, we will analyse the various shapes of possible DM signals. We will scan the M_T shapes or different $\Delta\phi$ and η distributions for example. After analysing the 'main' shape (M_T), we will do a full simulation of the process. With the help of this full simulation we will set expected limits as explained in section 5.2.1.

To analyse the shape of the processes in the AV model, we choose the min width approach (Γ^{min}_{med}). The reason is that it gives the best significances[13] due to the biggest cross sections. The reason why we do not analyse the shape for the other width approaches is to save computation time.

The first thing we want to look at is the M_T shape of the different signals. As visible in Fig. 21 for different g_q and Fig. 22 for different g_{DM}, a variation of the coupling strength does not change the shape and just scales the cross section of a process. It confirms the naive expectation that the biggest cross sections can be found in the processes with the biggest couplings. We will take a closer look on the specific structure between a coupling and the cross section in the next section.

In contrast to different coupling strengths the M_T shape changes with different mediator masses, see Fig. 23. To have a better sense, how the M_T shapes depend on the mediator masses, the distribution is additionally drawn normalized in Fig. 24.

As in the usual approach, we could now scan and fit the M_T shape to get a numerical measure to classify how the M_T shape depends on M_{med}. Exponential functions ($f(x) = [0]\cdot\exp([1]x)\cdot x^{[2]}$) can be fitted to the Monte Carlo data, to quantify the shape dependence from M_{med}, see Fig. 25 for the fits and Fig. 26 - Fig. 28 for the different fit parameters. As visible in Fig. 27 the M_T shape is mainly influenced in the exponential factor (fit parameter 1). The different mediator masses do not change the scaling of the different cross sections (see Fig. 26), within their uncertainties. Additionally no polynomial differences were observed (Fig. 28) for the signal shape. This fit is a tool to establish the influence from different parameters on the different measurable shapes. For different coupling strengths, we showed that the shapes are independent on g_q/g_{DM}. Just the 'fit parameter 0' depends on the coupling strength g_q/g_{DM}. This means that just the cross section scales for different coupling strength g_q/g_{DM}.

[12] A proper list of the scanned shapes, parameters and varied parameters in the cross section study can be found in the overview table in section 5.2.5.

[13] The significance is a measure, how well a possible DM signal could be observed above the signal background.

A scan to the full simulation data is performed on the M_T shape to set observation limits.

Above, we observed that the M_T shape just depends on the mediator mass M_{med}. Because of this, we know that a possible signal only depends on the mediator mass M_{med} as well. So we can determine, that the expected limits can be set mediator mass M_{med} dependent. Because the M_T does not depend on the coupling strength, the expected limits are coupling strength g_q/g_{DM} independent.

Now that we know how the M_T shape depends on the different model parameters, a full simulation with GEANT4 is done for different mediator masses. So we find exclusion limits for different luminosities dependent on the mediator mass M_{med}. The different integrated luminosities are chosen as described in section 5.2.1.

The following equation shows, how the number of measured events depends on the total event cross section σ_{Event} and the integrated luminosity L_{int} (collected data).

$$N = \sigma_{Event} \cdot L_{int}$$

The exclusion limits are visualized in Fig. 43 for the different integrated luminosities (1,30,300 and 3000 fb^{-1}).

These observation limits can be applied to the parameter plots (see later Fig. 56 - Fig. 61) in a further analysis.

Additionally the process can be studied for other parameters and observables. Scanning the number of processes with a W^+/W^- is possible. This reveals, that the processes, in which a W^+ is produced have roughly three times the quantity of the processes with a produced W^-. This results from the parton distribution function (PDF) (see Fig. 20). This PDF is the inner structure of protons which defines the ratio of the momentum that every subparticle of a proton contributes to the total proton momentum. The real quarks in the proton are 2 up quarks and 1 down quark, all the rest are sea quarks. Thus an event with positive charge in the final state is more likely to be produced. Due to this a lot more positrons and 'real' neutrinos than electrons and anti-neutrinos are produced in the final state.

Additionally a scan for other observables is done. As expected all the distributions are ϕ independent, see Fig. 35 - Fig. 40. The coupling strengths g_q/g_{DM} do not influence the η shapes (see Fig. 29 - Fig. 32) of the lepton and possible jets.

The mediator mass M_{med} influences the η shape of the lepton (see Fig. 33 - as we can see in the ratio plot, there is a structure dependent on the mediator mass). This effect lies within the uncertainties for this parameters. The mediator mass M_{med} does not influence the η shape of the jets (see Fig. 34).

Additionally we can check our expectations of the process. For example should the mediator recoil against the W boson as seen in Fig. 9.

As expected, the mediator and the W boson recoil against each other, what can be seen in a $\Delta\phi$(W,med) distribution (see Fig. 41). This is due to the fact that the overall transverse momentum in the detector has to stay zero.

The generator study also allows to look at non-detectables, such as the neutrinos. If we look at the $\Delta\phi$ between the neutrino and the W boson ($\Delta\phi$(W,neutrino)), as shown in Fig. 19, we find an imbalance of the neutrino direction considering the W (see Fig. 42):

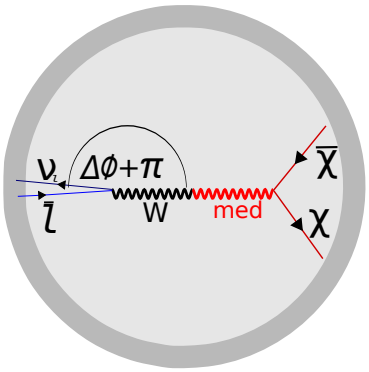

Figure 19: A schematic illustration for the angle $\Delta\phi$(W,neutrino). The detector is shown in a transverse plane.

The neutrino is more likely to recoil than to go straight in the W direction. This is pleasant on the experimental side. If the neutrino chooses to go into the opposite direction of the W boson, it goes into the direction of the MET. Because of this, the neutrino raises the MET. This results in better detectability. Studying this effect for different mediator masses reveals that it decreases with lower mediator masses and disappears for $M_{med} = 2 \cdot M_{DM}$. This behavior hints that it is a PDF effect. The mediator mass M_{med}'scans' the PDF of the proton.

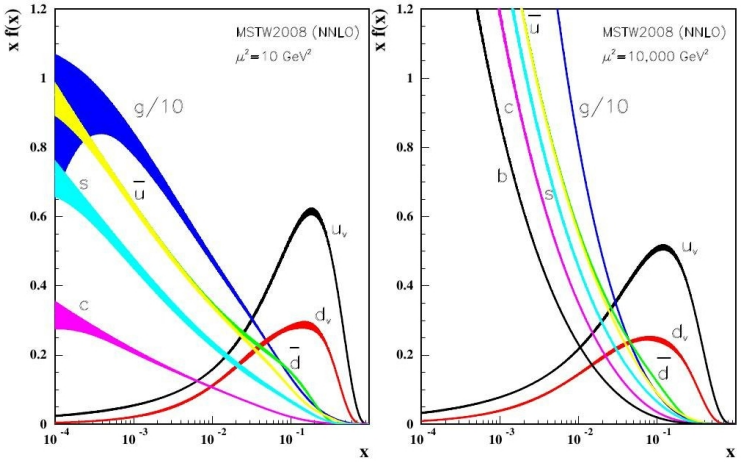

Figure 20: Distributions of x times the unpolarized parton distributions f(x) (where f = u,d,$\bar{u}$, $\bar{d}$,s,c,b,g) and their associated uncertainties. Done at a scale $\mu^2 = 10\,\mathrm{GeV}^2$ and $\mu^2 = 10000\,\mathrm{GeV}^2$. [23]

For bigger mediator masses, a lot smaller x in the PDF is reached, and seaquarks (c,s,b,t) get visible to the mediator. The structure of the $\Delta\phi$(W,neutrino) distribution comes from a polarization of the W boson. This effect is explained in the appendix.

The following plots show the M_T shape in the **AV** model for different parameters. The additional ratio plots show, that there is no difference (for different g_q and g_{DM}) in the shapes besides the scaling. The ratios are calculated with the first drawn distribution and all other distributions. The labeling has the following form: [varied parameter,normalized]

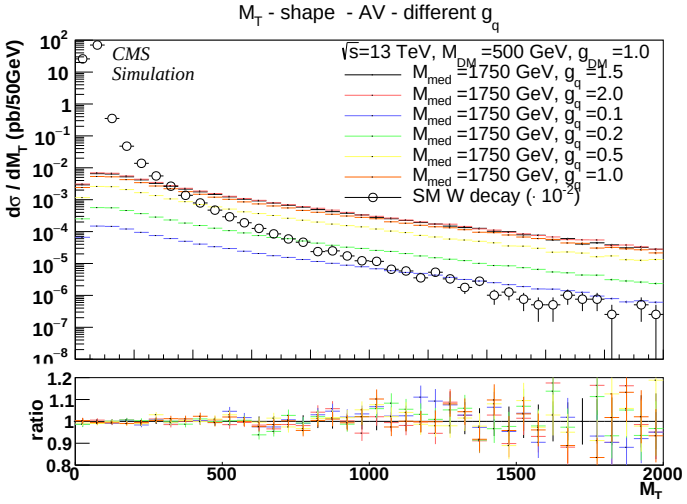

Figure 21: [g_q,not]

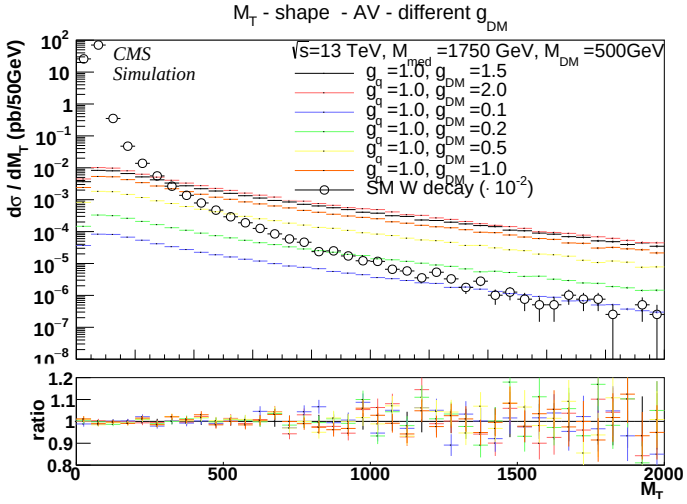

Figure 22: [g_{DM},not]

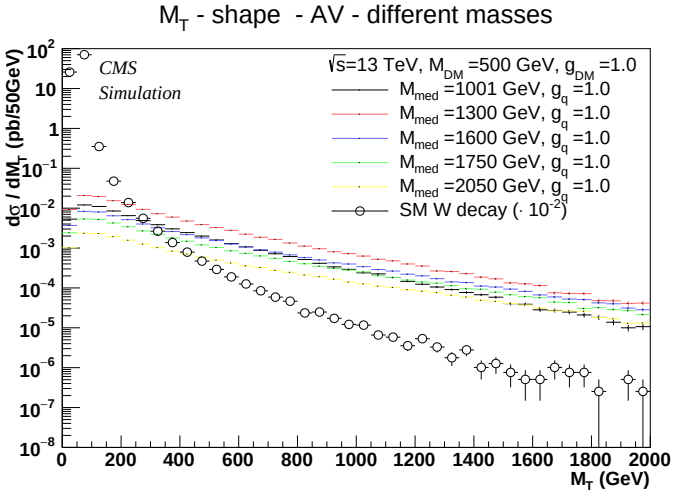

Figure 23: [M_{med},not]

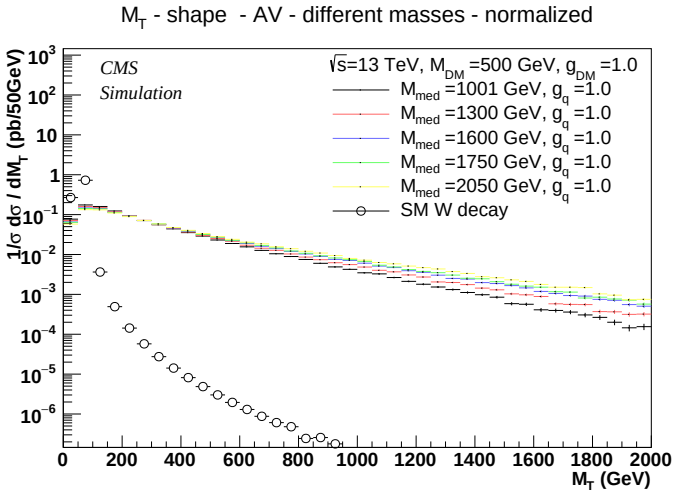

Figure 24: [M_{med},yes]

The following plots show an exemplary fit of a M_T shape in the **AV** that can be used to quantify the M_T shape dependence on one parameter (in this case M_{med}).

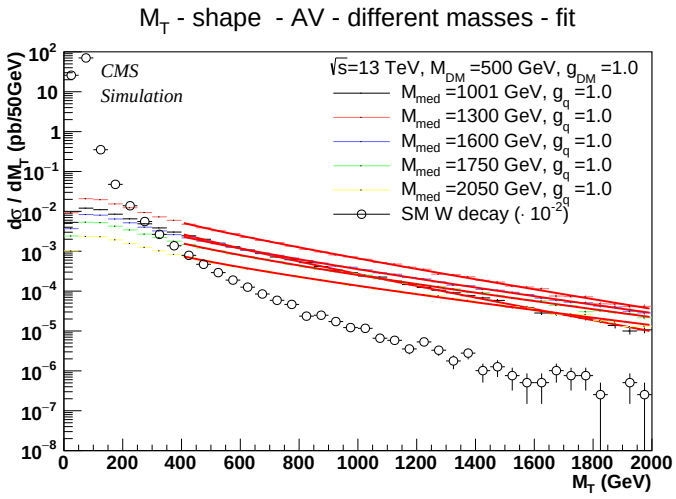

Figure 25: Various M_T shapes for different M_{med} with an exponential fit with $f(x) = [0] \cdot \exp([1]x) \cdot x^{[2]}$

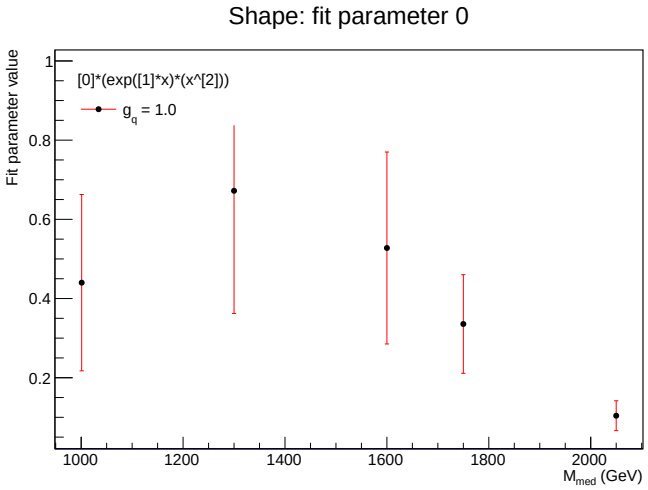

Figure 26: Fit Parameter 0

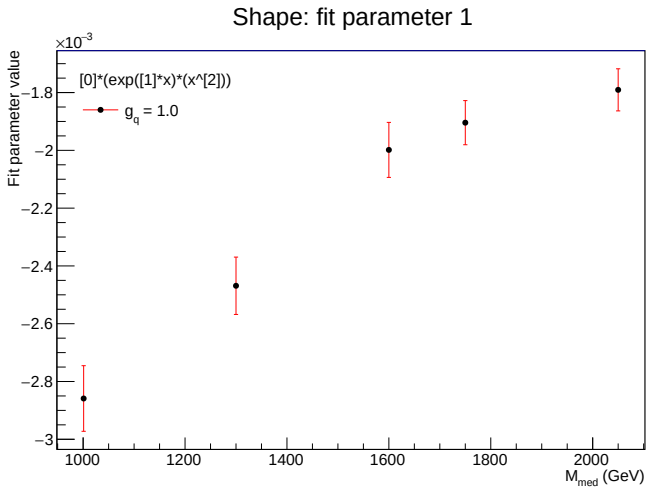

Figure 27: Fit Parameter 1

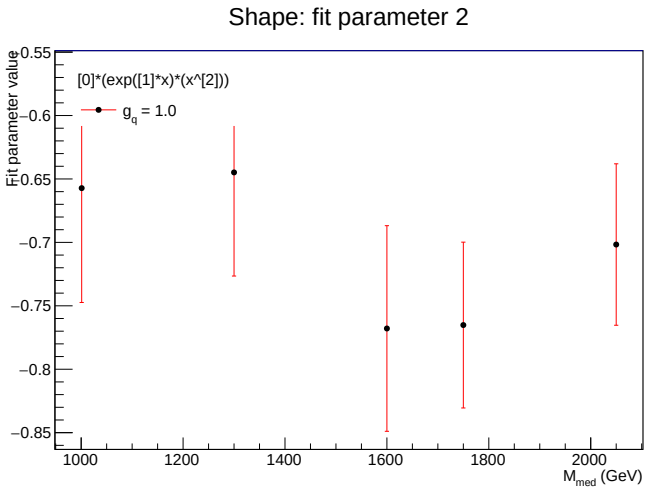

Figure 28: Fit Parameter 2

The following plots show the η shape in the **AV** model for different parameters. The appended ratio plots show the ratio of the distributions and the first drawn distribution (if the line at one is dotted) / the SM background (if the line is drawn through). The labeling has the following form: [particle,varied parameter,normalized]

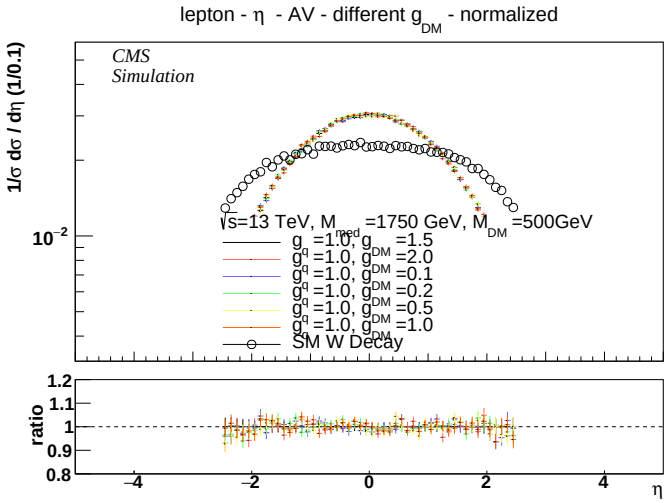

Figure 29: [lepton,g_{DM},yes]

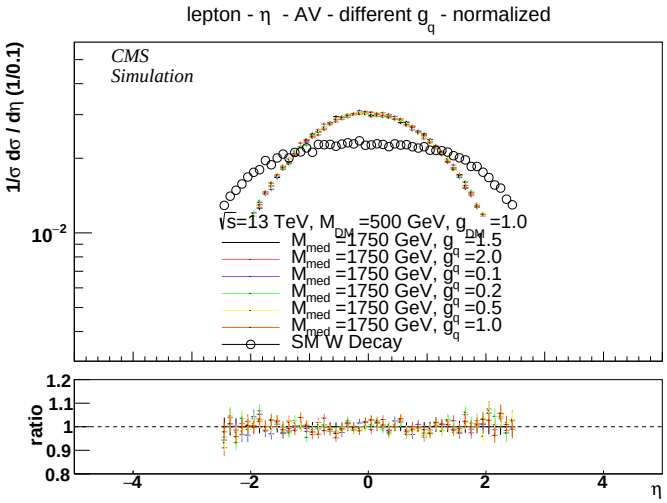

Figure 30: [lepton,g_q,yes]

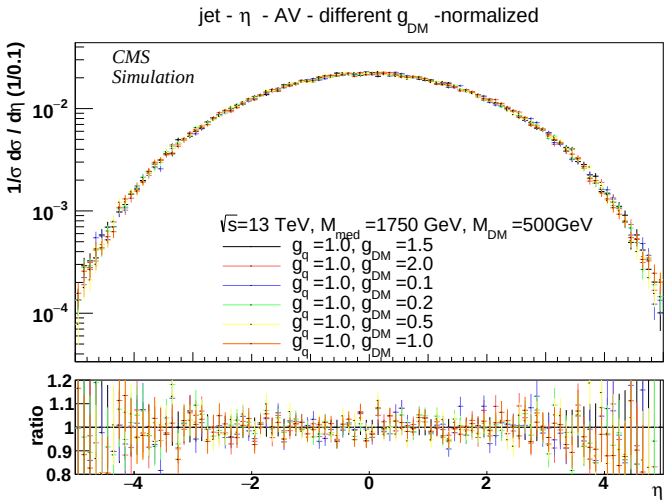

Figure 31: [jet,g_{DM},yes]

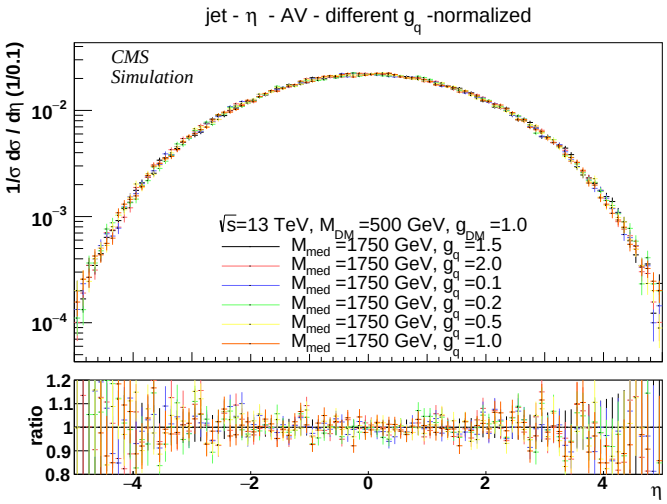

Figure 32: [jet,g_q,yes]

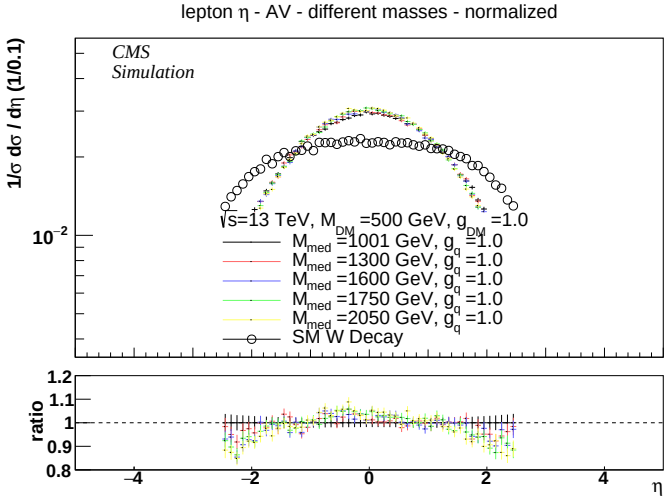

Figure 33: [lepton,M_{med},yes]

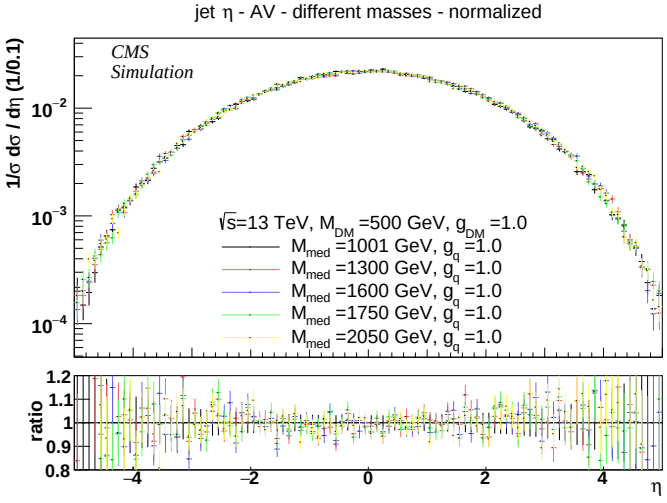

Figure 34: [jet,M_{med},yes]

The following plots show the ϕ shape in the **AV** model for different parameters. The appended ratio plots show the ratio of the distributions and the first drawn distribution (if the line at one is dotted) / the SM background (if the line is drawn through). The labeling has the following form: [particle,varied parameter,normalized]

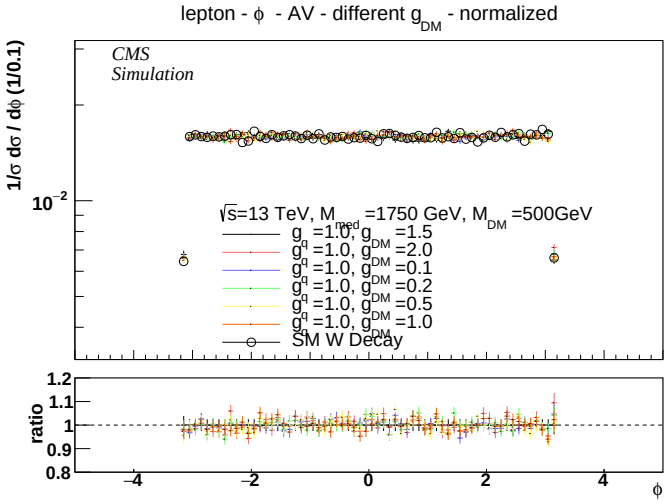

Figure 35: [lepton,g_{DM},yes]

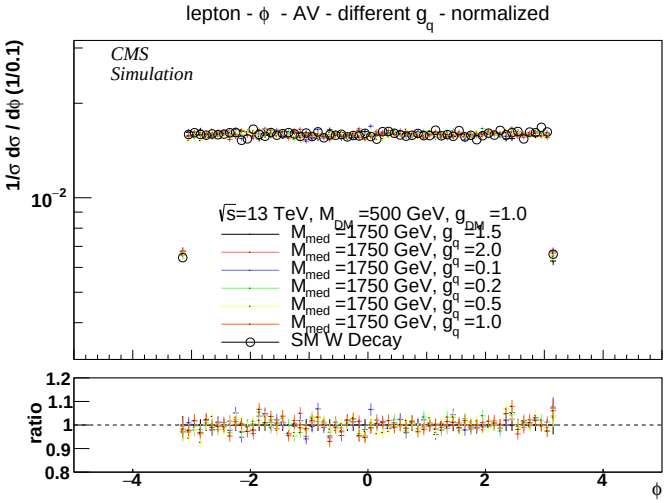

Figure 36: [lepton,g_q,yes]

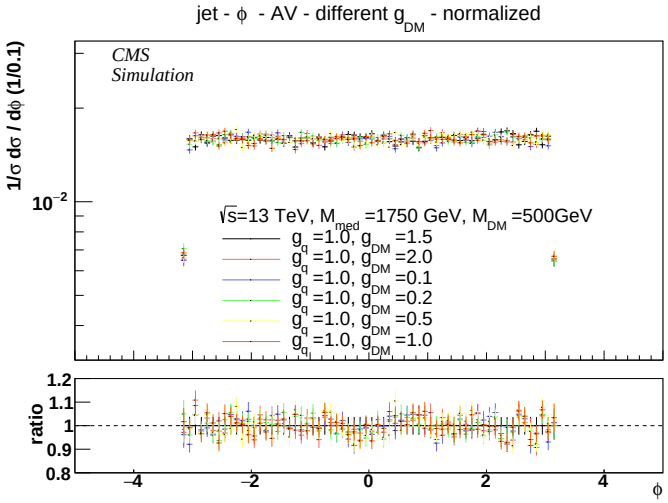

Figure 37: [jet,g_{DM},yes]

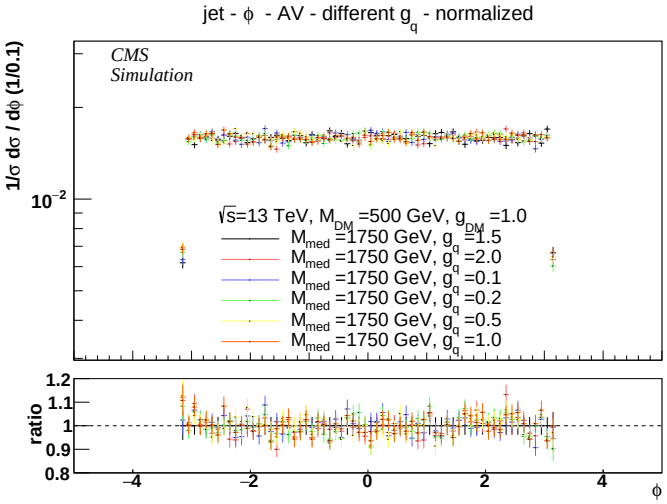

Figure 38: [jet,g_q,yes]

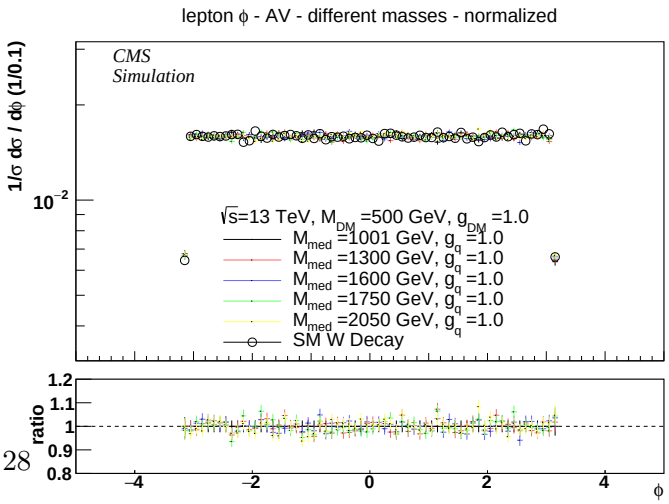

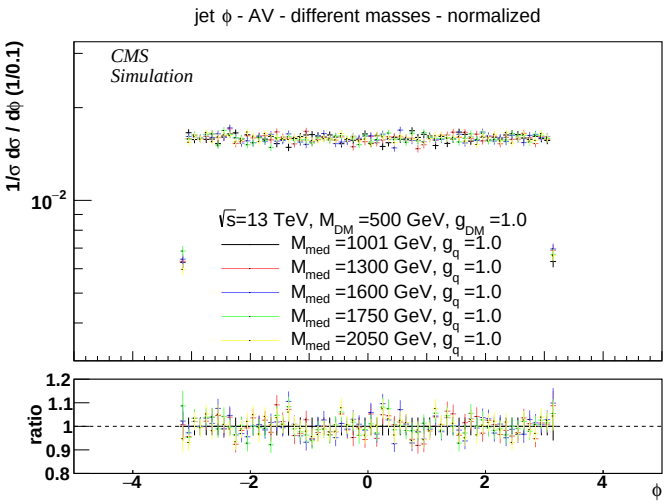

The following plots show additional distributions in the **AV** model for different M_{med}. The labeling has the following form: [distribution,varied parameter]

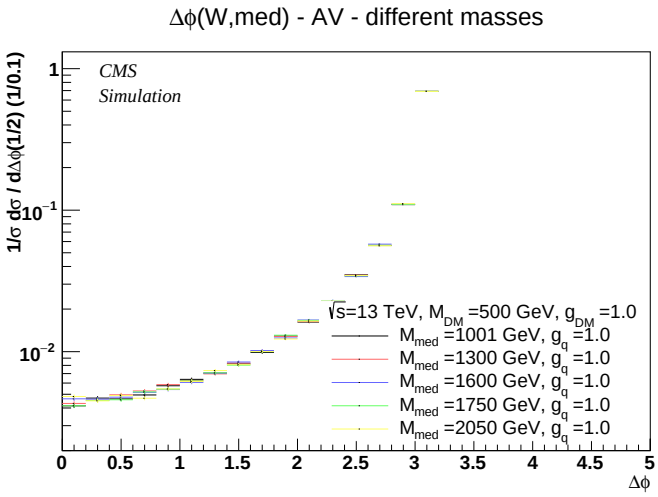

Figure 41: [$\Delta\phi$(W,med),M_{med}]

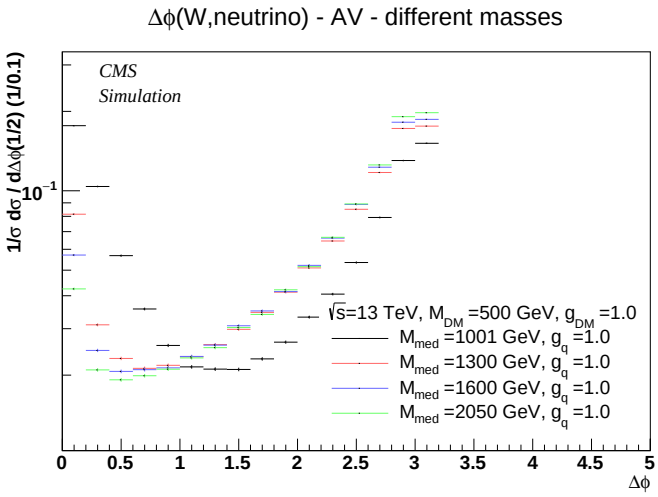

Figure 42: [$\Delta\phi$(W,neutrino),M_{med}]

The following plots show the expected limits in the **AV** model. These are generated with a GEANT4 full simulation. The limits are produced for integrated luminosities of (1,30,300 and 3000) fb^{-1}. The labeling has the following form: [model]

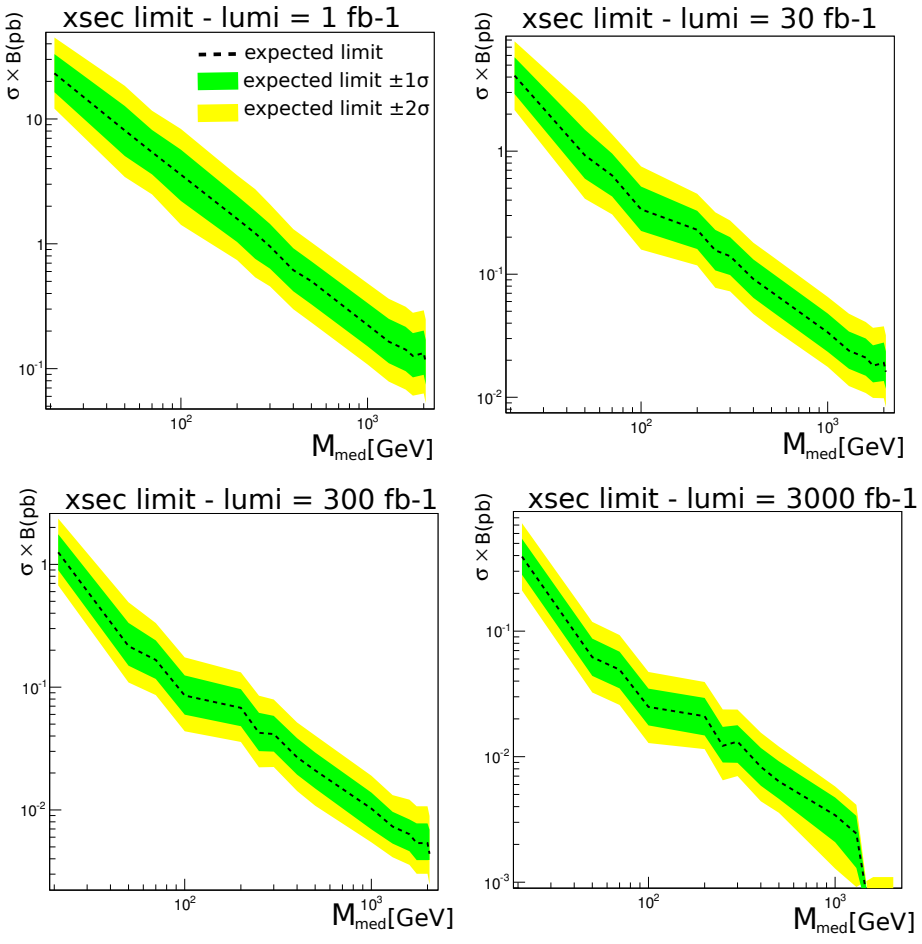

Figure 43: [AV]

6.1.2 Cross Section Analysis in the AV model

After analysing the signal shape and structure an analysis of the total process cross section in the AV model follows.

This analysis is split into three different parts for the three different width approaches ($\mathbf{\Gamma^{min}_{med}}$, $\mathbf{\Gamma^{full}_{med}}$ and $\mathbf{\Gamma^{Z}_{med}}$).

The reason why we scan the parameter space in respect to the full event cross sections is, that this shows which sensitivities each process has. A subsequent full simulation of the process can reveal the possible detector outcomes. With this procedure it is possible to exclude parts of the parameter space where we have not observed a signal.

6.1.2.1 Cross Section Analysis - $\mathbf{\Gamma^{min}_{med}}$ It has to be accepted, that for a discussion of events with high significances, the min width approach $\mathbf{\Gamma^{min}_{med}}$ that delivers the highest cross sections is the approach of choice. The min width approach provides the smallest possible widths for the mediator and due to this the highest possible cross sections. The mediator couples to one light quark with one color and the DM particle. In section 4.1 we saw, that the contributions to the value of the mediator width are almost [14] equal for matter and DM in this width approach.

First of all, we want to study the cross section dependence on the two coupling parameters (the coupling between the mediator and matter (g_q) and the coupling between the mediator and DM (g_{DM})) in particular. These scans are presented in Fig. 44 and Fig. 45.

It can be observed that the cross sections peak at a certain point and than decrease to lower values. The peak is reached for couplings of $g_q^{peak} \approx 2.5$ and $g_{DM}^{peak} \approx 3$.

This peak in the cross sections was naively not expected. The expectation was that the cross sections rise for increasing coupling strength (g_q/g_{DM}).

This observation means, that the cross sections decrease for raising coupling strengths. The two plots (Fig. 44 and Fig. 45) have been drawn in the usual parameter space of $0.1 < g_q$ and $g_{DM} < 2.0$ and additionally in a zoomed region. This has been done to observe the cross section peak for even bigger couplings ($g_{q^{peak}} > 2$ and $g_{DM}^{peak} > 2$)

Now we know that the cross sections show an unexpected behavior for raising coupling strengths. We now want to find out what causes this effect:

To find out why this peak occurs we will take a look at the dependence of the mediator width $\mathbf{\Gamma^{min}_{med}}$ on the couplings (g_q/g_{DM}). The width exclusion criterion ($\Gamma_{med} \overset{!}{\leq} M_{med}/3$) is drawn into the width plots (Fig. 50 and Fig. 51). As explained in section 4.1, this criterion delivers a comparison, at which point the NLO term is equal to the LO term. If the mediator width Γ_{med} raises above this constrain, the events are no longer physically motivated.

When studying the width in Fig. 50 and Fig. 51, we see that the width exclusion criterion is exceeded for couplings of $g_q \approx 2.0$ and $g_{DM} \approx 2.5$. For almost the same coupling strengths, the cross section in Fig. 44 and Fig. 45 peaks. This validates, that the events at the falling edge of the peak in Fig. 44 and Fig. 45 are nonphysical.

Those events are marked in the parameter plots (see Fig. 56 - Fig. 61).

The nonphysical behavior just occurs for high values of the couplings g_q and g_{DM}. This allows to study the coupling parameters $g_{q/DM}$ for high values and nevertheless cover big parameter sets in the following studies.

Now it is possible to look at different g_q and g_{DM}. We will do this in a 3D parameter plot (g_q |g_{DM}). To this parameter plot, we can apply the expected limits (see Fig. 43) and the width criterion ($\Gamma_{med} \overset{!}{\leq} M_{med}/3$) as mentioned above. This is done in Fig. 56. The width exclusion criterion for ($\Gamma_{med}/M_{med} > 1/3$) is just exceeded for very high very high coupling strength (see Fig. 50 and Fig. 51). It is not visible in the plot. The low width limit ($\Gamma_{med}/M_{med} < 1/8\pi$) shows, where ($\Gamma^{min}_{med} < \Gamma^{nar}_{med}$). This applies for $g_q \cdot g_{DM} < 1$.

[14] The contributions to the width for matter and DM just vary with the 'mass correction' term in the width formula. This mass correction term is highly suppressed by the mediator mass M_{med}.

The parameter observation limit plots cover a larger parameter space and give good significances in terms of attainable luminosities.

The parameter space can be scanned in big regions for luminosities of 300fb^{-1} and is fully covered for a high lumi (3000fb^{-1}) analysis. The significances are good in wide regions of the parameter space for luminosities of 300fb^{-1}. Every event in the scanned parameter space is significant for a luminosity of 3000fb^{-1}.

Due to almost the same branching ratios for same coupling strength ($BR(\text{med} \to \chi\bar{\chi}) \approx BR(\text{med} \to \text{q}\bar{\text{q}})$) , the contour plots look balanced in the $g_q - g_{DM}$-area. Only the first mass correction term varies for the branching ratios as seen in equation 4 and equation 5.

As can be seen from the structure of the cross sections in Fig. 56, after one coupling got dominant in the process, the event cross sections do not depend on the other coupling strength anymore.

After scanning the cross sections concerning different coupling strengths, we will observe how varying mediator or DM masses influence the event cross sections. Fig. 59 and Fig. 60 show the production cross sections for different mediator masses and coupling strengths g_q (Fig. 59) and g_{DM} (Fig. 59). Fig. 61 shows the production cross sections for different DM masses and coupling strengths g_q (Fig. 61).

Fig. 59 and Fig. 60 show that the mediator mass dependence of the cross sections is very high. A second significant fact is that the cross sections decrease for mediator masses close to twice the DM mass and thus a total on-shell production. This was expected.

No strong dependence on the DM mass can be observed in Fig. 61. For heavy DM particles, where it comes to off-shell production, the cross sections decrease rapidly.

6.1.2.2 Cross Section Analysis - $\mathbf{\Gamma^{full}_{med}}$

This model ($\mathbf{\Gamma^{full}_{med}}$) describes a mediator, that couples to all quarks with all colors and to the DM particle.

Because the coupling to the quarks is more numerous here, the branching ratio to the quarks BR(med $\to \bar{q}q$) is a lot bigger than the branching ratio to the DM particle BR(med $\to \bar{\chi}\chi$) for same strenghts of the couplings ($g_q = g_{DM}$). This is the results of the fact that the coupling structure for med$\leftrightarrow$matter and med$\leftrightarrow$DM are the same. The proportion of the branching ratios ($BR(\text{med} \to \text{q}\bar{\text{q}})/BR(\text{med} \to \chi\bar{\chi})$ [15] for same coupling strenghts is $\approx 1/18$, if the mass correction term (see equation 4 and equation 5) has not been taken into account[16].

First a cross section scan for one parameter at a time is done. Scanning the cross section dependencies from the parameters shows the behavior seen in Fig. 46 and Fig. 47. Looking at the g_q dependence (Fig. 46) reveals that the cross sections first raise for raising couplings what one would naively assume. But the cross sections peak at a certain point and decrease for a raising coupling strength g_q. It is significant that this peak can be found at very low coupling strengths ($g_q \approx 0.5$) on the matter side (g_q). This structure can be found for different g_{DM} for much higher values only ($g_{DM} > 2.0$), this is because of the lower branching ratio to DM.

To explain this behavior of the cross sections, we again take a closer look on the mediator width $\mathbf{\Gamma^{full}_{med}}$ in dependence of the different parameters. This scan can be seen in Fig. 52 and Fig. 51. Remarkable is the behavior in Fig. 51. If the coupling on the matter side is too high, the mediator width does not get smaller than $\Gamma_{med}/M_{med} > 1/3$ even for very low couplings on the DM side.

The cross section peak in Fig. 46 and Fig. 47 is on the same scale as the point where the width raises above the exclusion criterion ($\Gamma_{med}/M_{med} > 1/3$), see Fig. 52 and Fig. 51. This verifies that the peaking cross sections come from too large widths and a then failing perturbation theory in our model.

[15] This is the proportion of the mediator decaying into DM to the mediator decaying into matter.

[16] As seen in the two equations mentioned above, the mass correction term gets really small for small particle masses (M_q and M_{DM}). It is suppressed by the mediator mass M_{med}. Due to this it can be ignored in an estimation of the branching ratios.

We see that the width exclusion limits suppresses a possible discovery because it delivers strong parameter bounds in the naive approach. The main reason here is the failing perturbation theory for to large widths ($\Gamma_{\text{med}}/M_{\text{med}} > 1/3$). The generated events are not valid anymore in a physically encouraged way.

Due to this 'validity' only a few events can be analysed in the full width ($\Gamma^{\text{full}}_{\text{med}}$) approach.

This 'validity' can be applied to the 3D parameter plots as in Fig. 57. Just the events with a very low g_q are physical.

This approach is the least visible due to the lowest cross sections and the parameter bounds due to the width exclusion criterion.

The observation limits from section 6.1.1 are not applied to the parameter contour plot, because the observation limits in Fig. 43 are done for the min width approach ($\Gamma^{\text{min}}_{\text{med}}$), that has a totally different width. The observation limits are just valid for a model with a similar shape. The shape dependence on the mediator width is yet unclear and has to be discussed in further studies.

6.1.2.3 Cross Section Analysis - $\Gamma^{\text{Z}}_{\text{med}}$

To get a comparison width an other width approach, the same analysis is done for the $\Gamma^{\text{Z}}_{\text{med}}$ width case. Scanning the cross sections against a single parameters shows the deviations in Fig. 48 and Fig. 49. These cross sections are similar to those from the first discussed width model in section 6.1.2.1.

Scanning the widths for a single parameter shows the behaviours in Fig. 54 and Fig. 55. The cross section and width behave almost similar to the first model. Just the fraction of the branching ratios changes and gives an imbalance in the 3D cross section parameter plot (see Fig. 58). Again the width exclusion criterion can be drawn into the parameter cross section plot. Additionally we can apply the expected limits from the $\Gamma^{\text{min}}_{\text{med}}$ case to the parameter cross section plot as in Fig. 58. This is possible due to almost the same widths $\Gamma^{\text{min}}_{\text{med}}$ and $\Gamma^{\text{Z}}_{\text{med}}$. Because of this, the shapes of the min width and the Z width approach are similar. The same applies to the expected limits.

As visible, the parameter space can be scanned in big regions for luminosities of 300fb^{-1} and is fully covered for a high lumi (3000fb^{-1}) analysis.

The similarities between the $\Gamma^{\text{min}}_{\text{med}}$ and the $\Gamma^{\text{Z}}_{\text{med}}$ model show that totally different mediator width approaches than the already discussed ones (a fermionic width approach - see equation 4 and equation 5) are possible on the experimental point of view.

The following plots show the cross section dependence on different parameters in the **AV** model. The plots are done for all three different width approaches in the AV model. The labeling has the following form: [varied parameter,width approach]

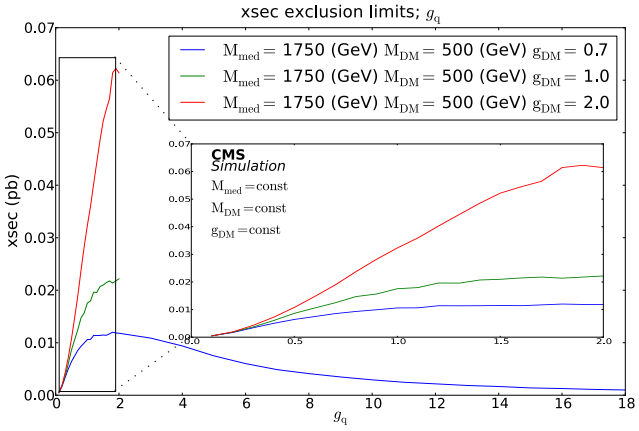

Figure 44: [g_q,Γ_{min}]

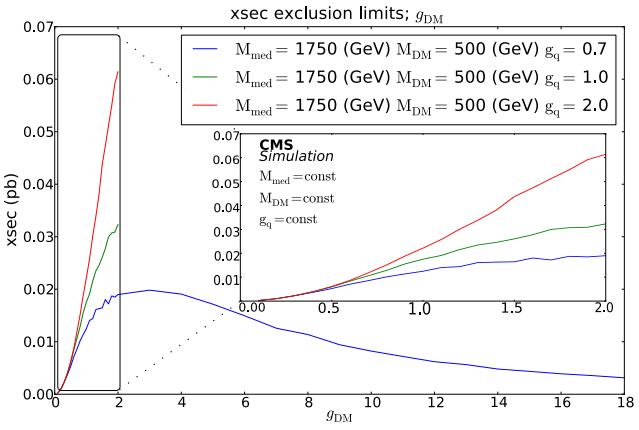

Figure 45: [g_{DM},Γ_{min}]

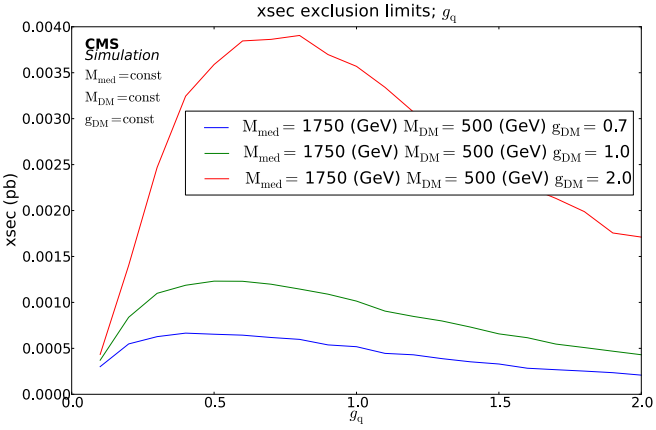

Figure 46: [g_q,Γ_{full}]

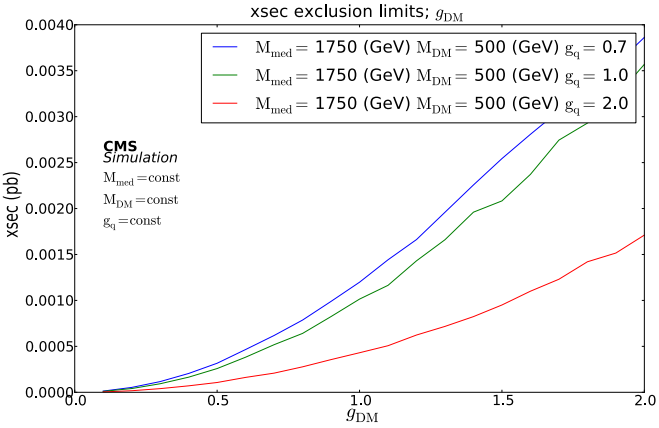

Figure 47: [g_{DM},Γ_{full}]

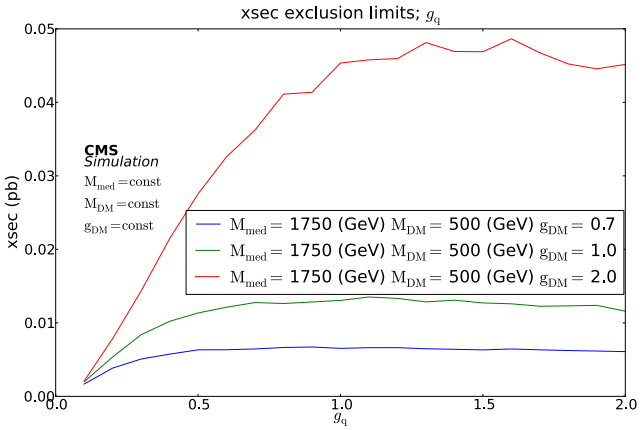

Figure 48: [g_q,Γ_Z]

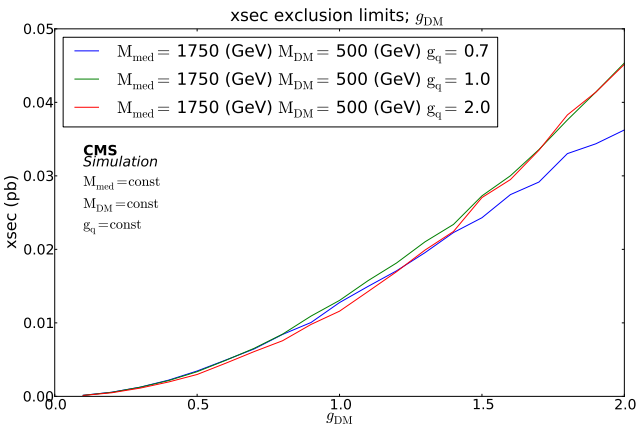

Figure 49: [g_{DM},Γ_Z]

The following plots show the width dependence on different parameters in the **AV** model. The plots are done for all three different width approaches in the AV model. The dotted line shows the width exclusion criterion of $\Gamma_{\text{med}} \overset{!}{\leq} M_{\text{med}}/3$.
The labeling has the following form: [varied parameter,width approach]

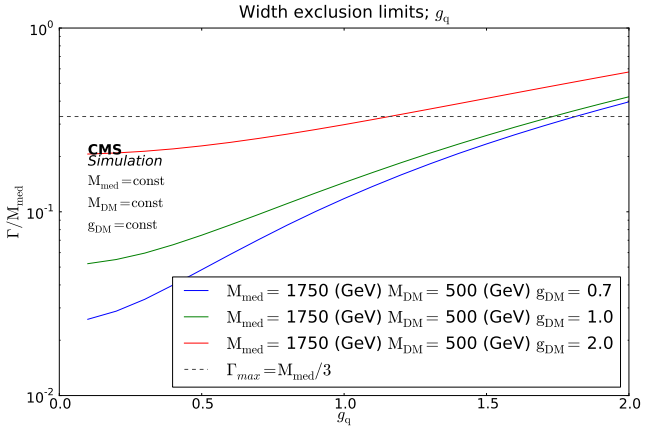

Figure 50: $[g_q,\Gamma_{\text{min}}]$

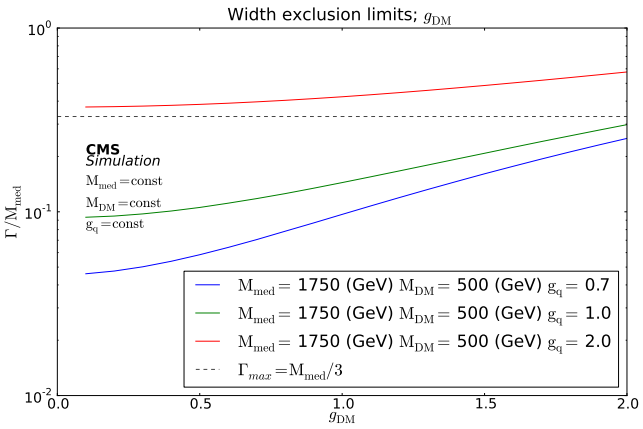

Figure 51: $[g_{DM},\Gamma_{\text{min}}]$

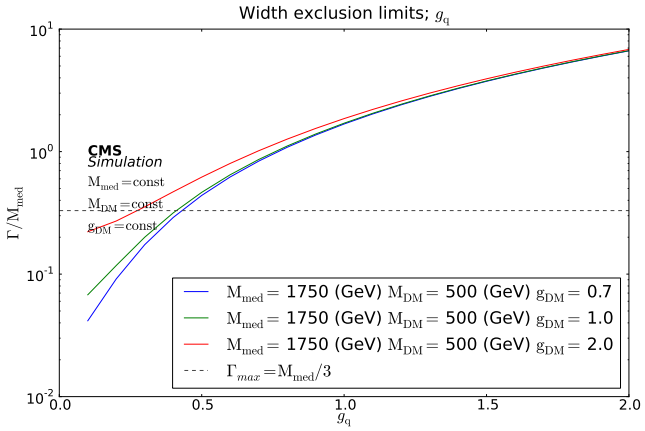

Figure 52: $[g_q,\Gamma_{\text{full}}]$

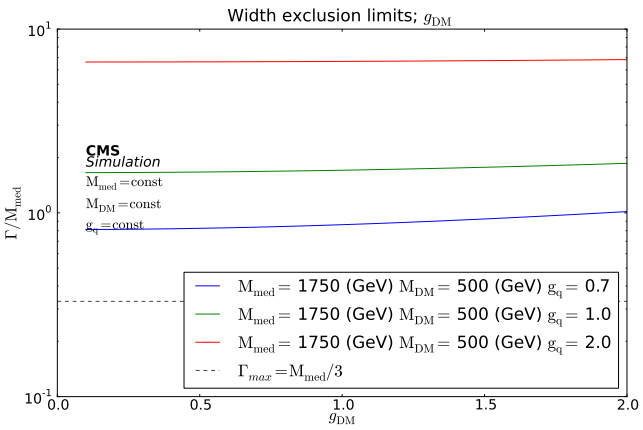

Figure 53: $[g_{DM},\Gamma_{\text{full}}]$

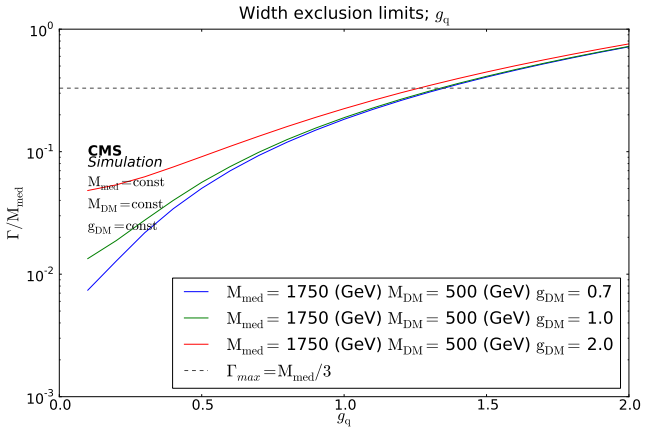

Figure 54: $[g_q,\Gamma_Z]$

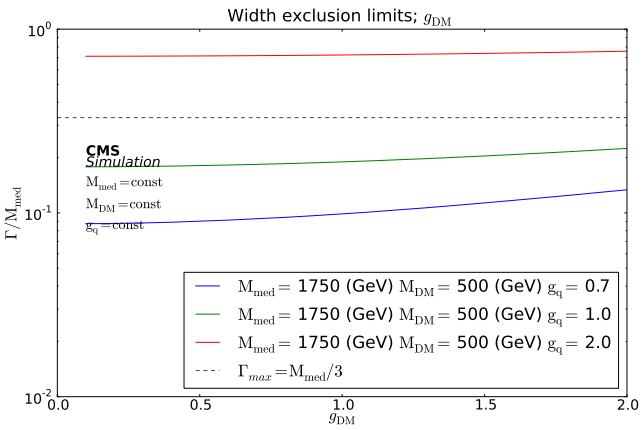

Figure 55: $[g_{DM},\Gamma_Z]$

The following plots show the cross section dependence on two parameters in each plot. The parameters are varied in the two dimensional grids introduced in table 3. The dotted lines are the expected limits transferred from Fig. 43. Additionally the width exclusion criterion of $\Gamma_{med} \overset{!}{\leq} M_{med}/3$ is added to the plots.
The labeling has the following form:
[first varied parameter | second varied parameter,model,width approach]

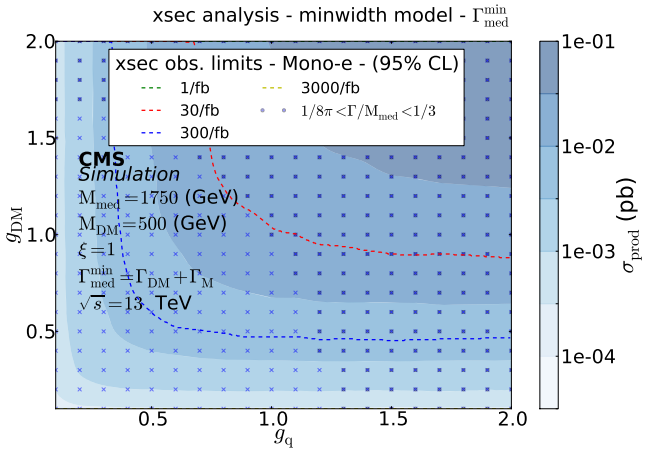

Figure 56: [g_q | g_{DM},AV,Γ_{min}]

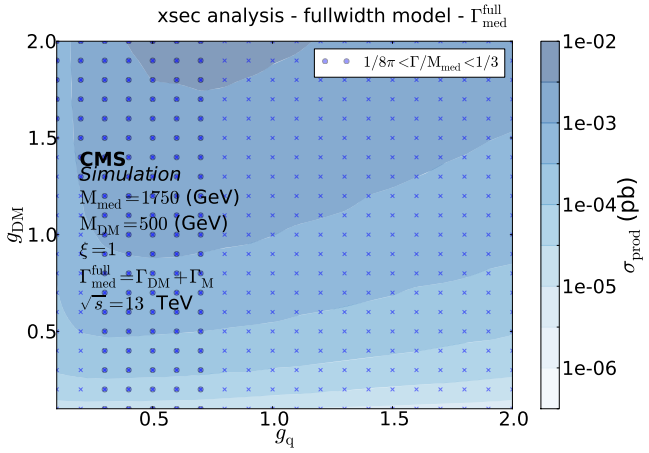

Figure 57: [g_q | g_{DM},AV,Γ_{full}]

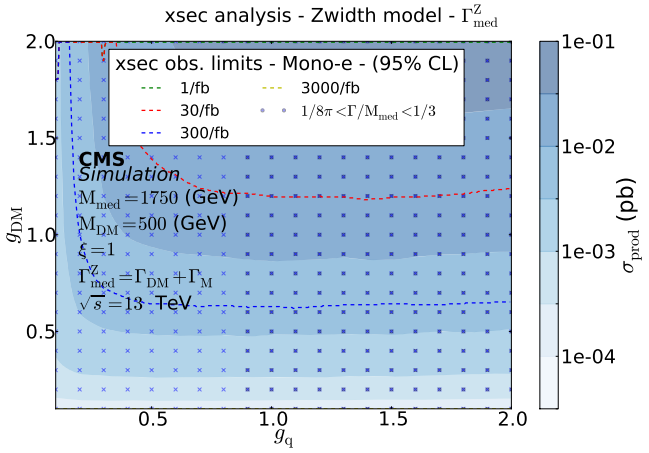

Figure 58: [g_q | g_{DM},AV,Γ_Z]

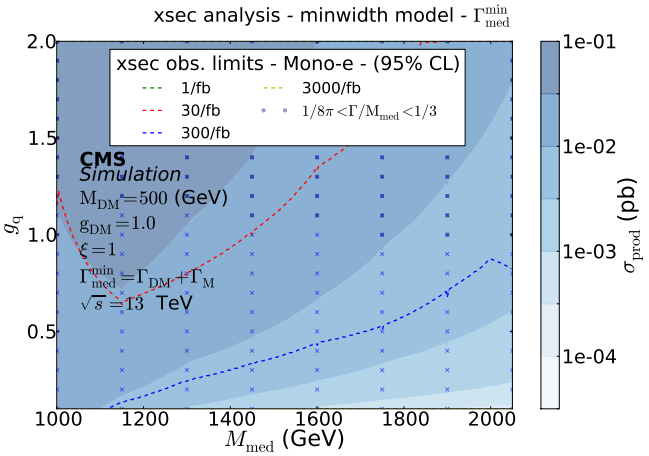

Figure 59: [M_{med} | g_q,AV,Γ_{min}]

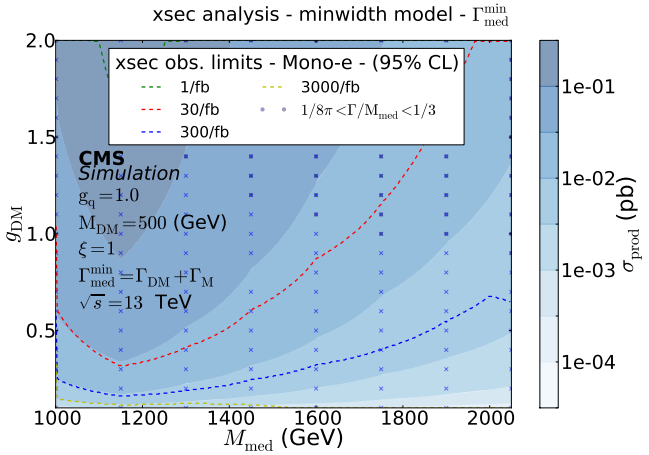

Figure 60: [M_{med} | g_{DM},AV,Γ_{min}]

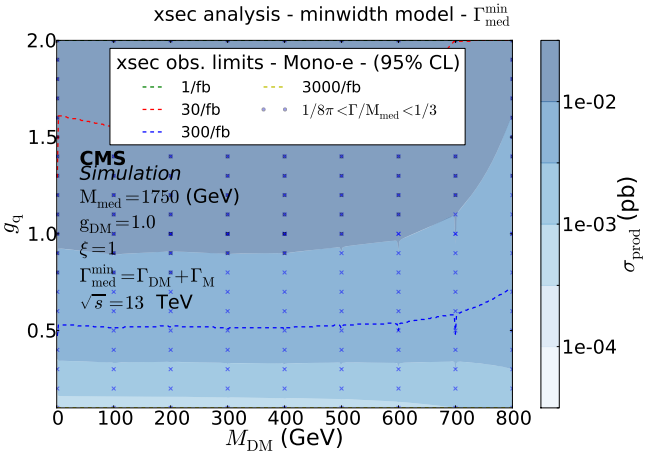

Figure 61: [M_{DM} | g_q,AV,Γ_{min}]

6.2 Scalar Model (S)

We will now take a look at the completely new model of a scalar coupling mediator. Once more we want to discuss the shape of the signal first and do a cross section analysis subsequently.

Because it is not implemented in the JHUGen yet to decay DM directly (as described in section 5.2), we can just scan the cross sections for different mediator masses and couplings with the generator output. Additionally as described in section 5.2.4 and section 5.2.5, the parameterspace for M_{med} is reduced due to two computation reasons. In this model, the coupling strength of med $\longleftrightarrow$ DM is always set on $g_{DM} = 1$ and the DM mass is fixed to $M_{DM} = 10\,\text{GeV}$. Because it is not possible to vary the mediator width like in the AV model, a narrow width approach ($\Gamma_{med} = M_{med}/8\pi$) is chosen.

This narrow width approach produces the best significances but it must be treated with caution because of exactly this reason. The physical sense of a narrow width approach has to be discussed before making such an assumption.

6.2.1 Shape Analysis in the S Model

We will now do a shape analysis in the S model for different M_{med} and g_W. This shape analysis is performed for the parameter sets introduced in table 5. The restrictions to the scannable parameter space have been discussed in section 5.2.4 and section 5.2.5.

Just like in the AV case, the M_T shape does not change for different coupling strengths (g_W) in the S model as we can see in Fig. 62. In a further analysis, a difference in the M_T shape for different mediator masses (M_{med}) can be found. This is visible in Fig. 63.

Compared to the background the M_T shape is similar. Because of this, a scan of this shape would probably not provide the best significances in terms of a discovery, when assuming a S model for the mediator.

Additionally also a scan for other observables is done. As expected all the distributions are ϕ independent in the S model as well what can be seen in Fig. 66 and Fig. 67. The η shape stays the same for different g_W as seen in Fig. 64.

It is very interesting that the η shape of the lepton as seen in Fig. 65 varies for different mediator masses. We have seen this behavior in the AV model yet at a low scale. For very light mediators ($M_{med} < 50\,\text{GeV}$), the η shape is different to the W background in the outer η regions ($\eta < -2$ and $\eta > 2$). Nevertheless this distribution shows simulated data at generator level. Looking at the η shape after a full simulation and with respect to the possible detector resolution would be necessary to make a statement about the possible usage of η as a discrimination observable.

No jets are radiated in this model we could scan on, see section 5.1.2. The p_T^{lep}/p_T^{MET}-distribution peaks at one as expected. Fulfilling expectations the mediator and the W boson recoil against each other in the S model as well. Because of no present jets, the $\Delta\phi$(W,med) distribution is exactly peaking at π (see Fig. 68)

We have seen above that the main scanning shape, the M_T shape, just changes for different M_{med}. Thus a full simulation with GEANT4 is done for different mediator masses, and rends exclusion limits for different luminosities dependent on the mediator mass M_{med}. The results are visualized in Fig. 69.The exclusion limits are produced for mediator masses $M_{med} < 200\,\text{GeV}$ only. They will be extrapolated for mediator masses $M_{med} > 200\,\text{GeV}$. This is reasonable due to the smooth shape.

The following plots show the M_T shape in the **S** model for different parameters. The additional ratio plot shows, that there is no difference (for different g_W) in the shapes besides the scaling. The ratio is calculated with the first drawn distribution and all other distributions. The labeling has the following form: [varied parameter,normalized]

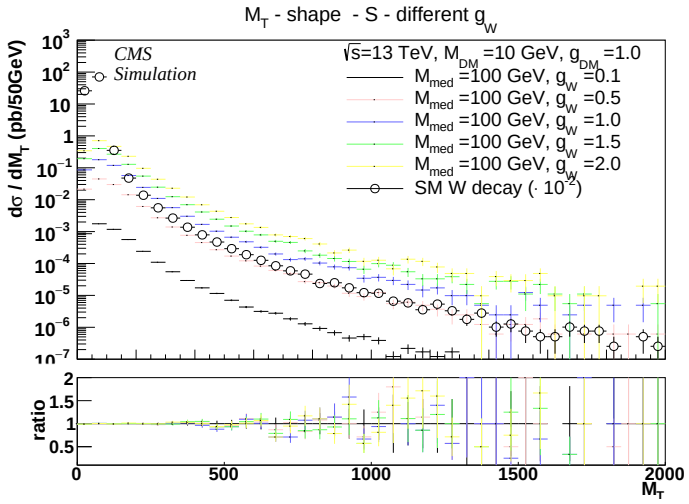

Figure 62: [g_W,not]

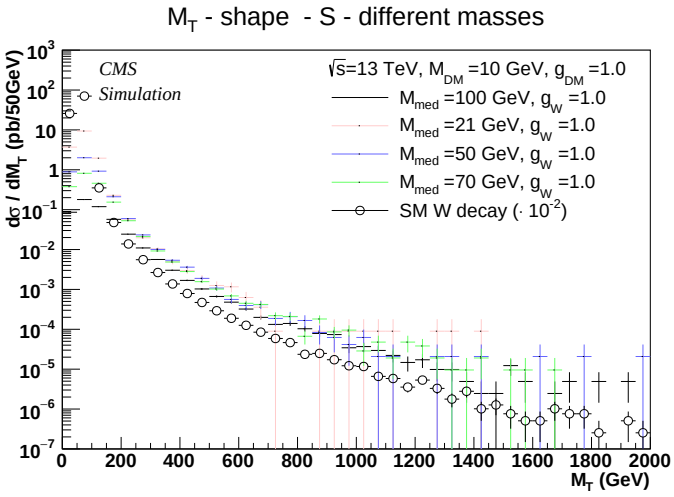

Figure 63: [M_{med},not]

The following plots show the η shape of the lepton in the **S** model for different parameters. The appended ratio plots show the ratio of the distributions and the first drawn distribution (if the line at one is dotted) / the SM background (if the line is drawn through). The labeling has the following form: [varied parameter,normalized]

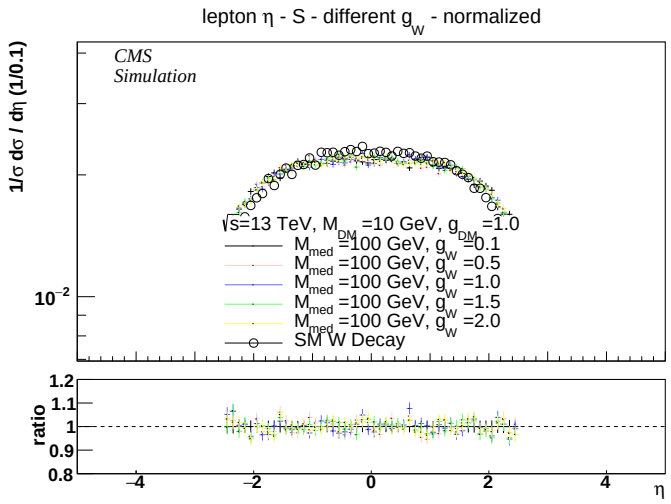

Figure 64: [g_W,yes]

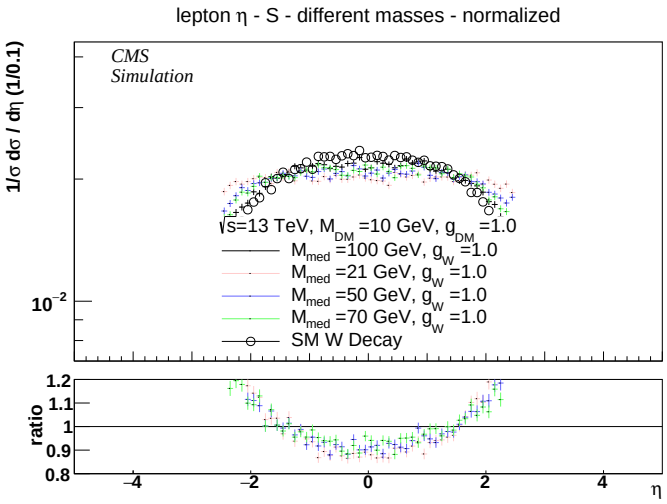

Figure 65: [M_{med},yes]

The following plots show the ϕ shape of the lepton (ϕ_{lep}) and the $\Delta\phi$(W,med) shape in the **S** model for different parameters. The appended ratio plots show the ratio of the distributions and the first drawn distribution (if the line at one is dotted) / the SM background (if the line is drawn through). The labeling has the following form: [distribution,varied parameter,normalized]

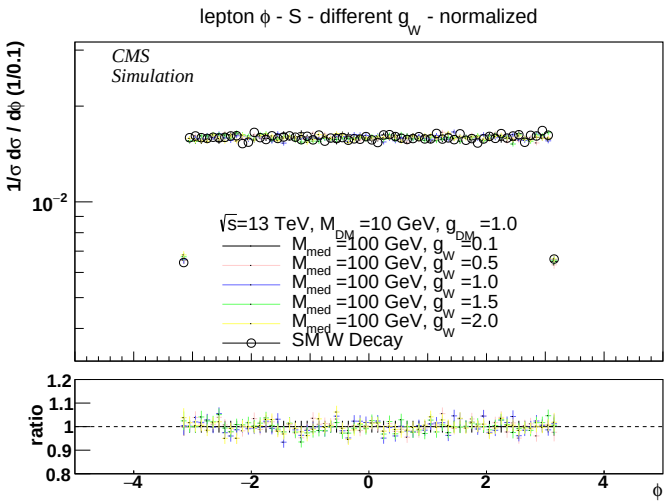

Figure 66: [ϕ_{lep},g_W,yes]

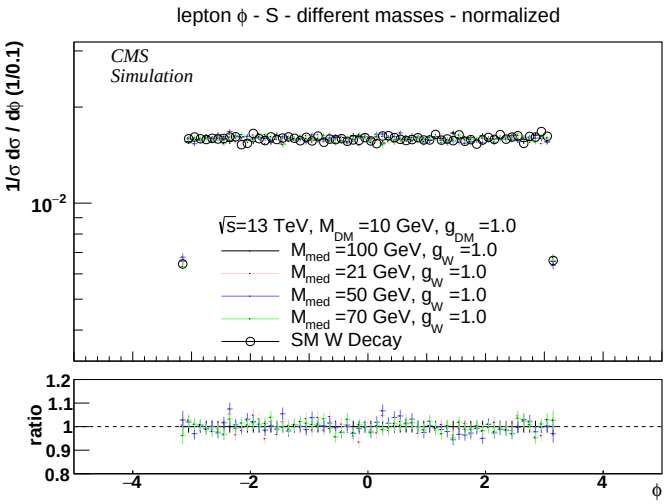

Figure 67: [ϕ_{lep},M_{med},yes]

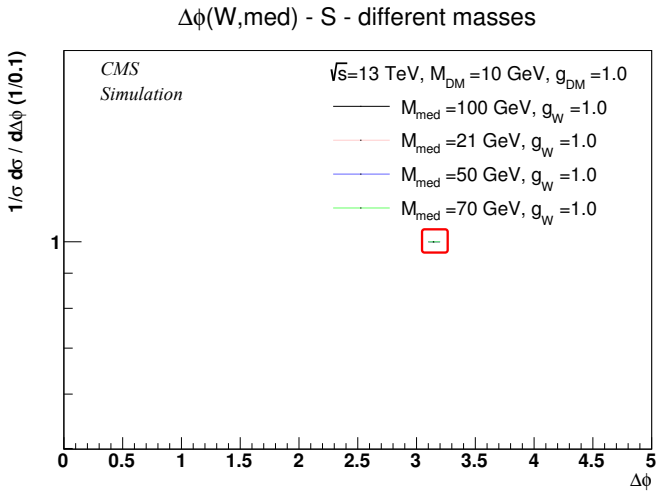

Figure 68: [$\Delta\phi$(W,med),M_{med},yes]

The following plot shows the expected limits in the **S** model. These are generated with a GEANT4 full simulation. The limits are produced for integrated luminosities of (1,30,300 and 3000) fb^{-1}. The labeling has the following form: [model]

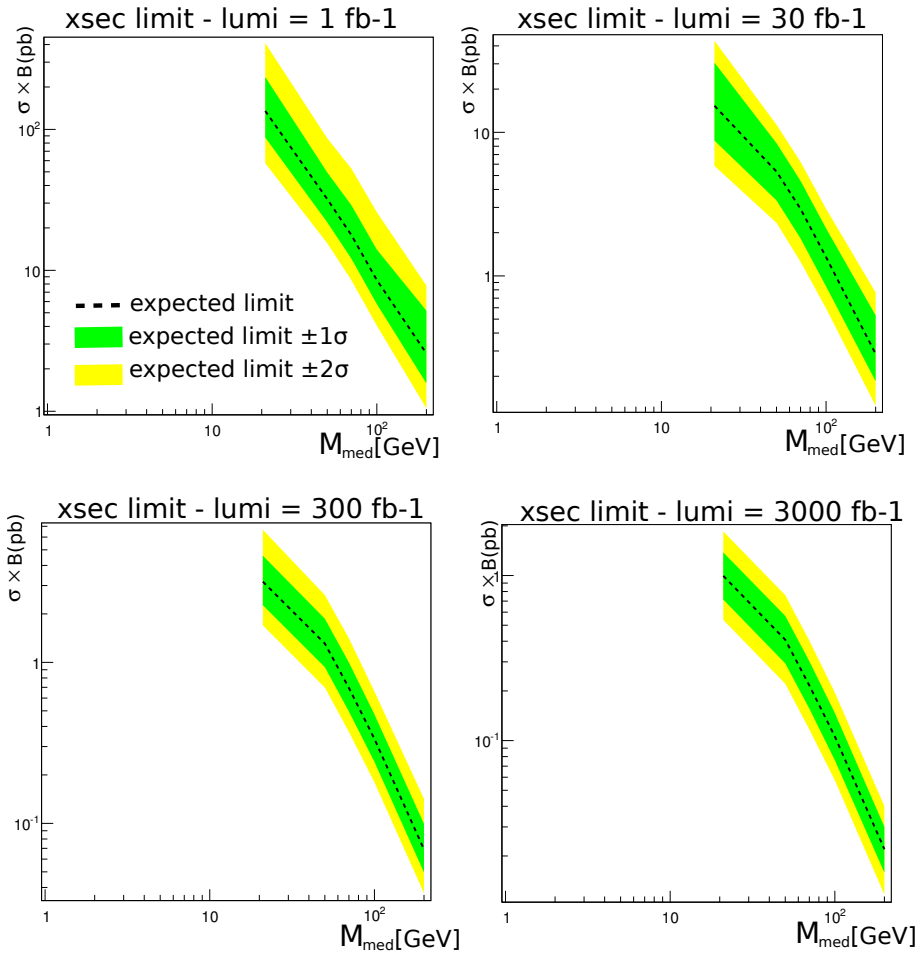

Figure 69: [S]

6.2.2 Cross Section Analysis in the S Model

After analysing the shape in the S model and producing observation limits (Fig. 69), as seen above, we can now scan the processes concerning the event cross sections. The parameters can be varied in the parameter steps, seen in table 5. For the different generated processes, the cross sections are put into a 3D histogram. The cross section scan of the scalar model is shown in Fig. 70. This reveals the influence of the parameters on the process.

It is visible that the range, in which the cross section raises, is 11 orders ($10^{-9} - 10^{1}$ pb) in the used parameter boundaries. This is a large cross section range. On the one hand this is good, because it produces big cross sections for some parameter sets, on the other hand the cross sections decrease very fast for changing parameters.

Additionally the cross section is very dependent on the chosen parameters. Especially a huge $\mathrm{M_{med}}$ dependence is found.

The expected limits show that for small mediator masses, observations could be possible for even small luminosities ($30\mathrm{fb}^{-1}$). To fully scan the process for higher mediator masses ($\mathrm{M_{med}} > 150\,\mathrm{GeV}$) high lumi is needed.

For medium large mediator masses of $\mathrm{M_{med}} > 150\,\mathrm{GeV}$ a possible discovery is strongly suppressed by the small cross sections of the events. A signal here (in a region of $\mathrm{M_{med}} > 150\,\mathrm{GeV}$)

is invisible even for very high luminosities ($> 3000\text{fb}^{-1}$) due to the semi outstanding M_T shape as mentioned in section 6.2.1.

The scalar model is not the best for a DM search because the significances decrease to strong for medium heavy mediators (in a region of $M_{med} > 150\,\text{GeV}$). A discovery is possible only for very light mediators.

The following plot shows the cross section dependence on two parameters. The parameters are varied in the two dimensional grids introduced in table 3. The dotted lines are the expected limits transferred from Fig. 69. Additionally the width exclusion criterion of $\Gamma_{med} \overset{!}{\leq} M_{med}/3$ is added to the plots.
The labeling has the following form:
[first varied parameter | second varied parameter,model,width approach]

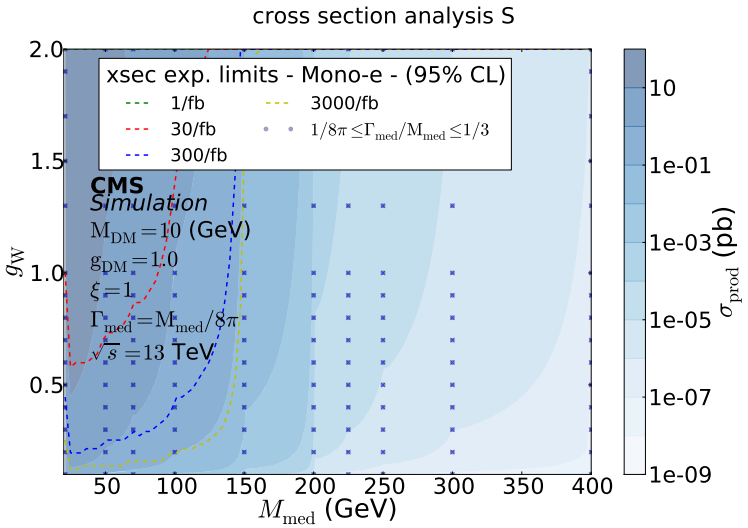

Figure 70: [M_{med} | g_W,S,Γ_{nar}]

6.3 Pseudoscalar Model (PS)

Now the same scan as for the two discussed models should be done for the PS model at last. First a shape analysis of the signal is performed and subsequently a cross section analysis for different model parameters.

The PS has the same computation difficulties like the S because the events are generated with the same generator (JHUGen). Therefore, the same assumptions about the mediator width and the DM particle are chosen. The scans are done for different mediator masses and varying g_W only. The coupling med $\longleftrightarrow$ DM is always set on $g_{DM} = 1$ and the DM mass is fixed to $M_{DM} = 10\,\text{GeV}$.

6.3.1 Shape Analysis in the PS Model

Just like in the AV and the S case, the M_T shape does not change for different coupling strengths (g_W) in the PS model as we can see in Fig. 71. In a further analysis, a difference in the M_T shape for different mediator masses (M_{med}) can be found, see Fig. 72.

Compared to the background the M_T shape is different. This way scanning to this shape would provide a fair scanning method to search in this channel. The largest shape deviations from the single W background occur for large mediator masses (Fig. 72). This is explained by a much bigger influence of the DM production to the process for bigger mediator masses. On the

other hand it is visible in section 6.3.2 that processes with large mediator masses produce the smallest cross sections and due to this do not provide good significances.

Additionally a scan for other observables is performed. As expected all the distributions are ϕ independent in the PS model as visible in Fig. 75 and Fig. 76. The coupling strength difference does not influence the η shapes of the lepton, see Fig. 73. What is more outstanding, is that in Fig. 74 it is visible, that the η shapes differ for other mediator masses just like in the S model. For very heavy mediators ($M_{med} < 50\,GeV$), the η shape is different to the W background in the inner η regions ($-1 < \eta < 1$). Due to the fact that the data is on generator level this shape difference may be not visible in the detector. Further studies could check the sensitivities here.

There are no jets in this model we could possibly scan on as explained in section 5.1.2. Additionally we took a look at the p_T^{lep}/p_T^{MET}-distribution, it peaks at one just as expected. As expected, the mediator and the W boson recoil against each other to 100% (see Fig. 77). The reason for this is that the mediator and the W are the only two particles on a generator level. They have to recoil against each other to conserve the transverse momentum before further decaying.

A full simulation with GEANT4 is done for different mediator masses, and rends exclusion limits for different luminosities dependent on the mediator mass M_{med}. The results are visualized in figure 78. The exclusion limits are produced for mediator masses $M_{med} < 200\,GeV$ only. They will be extrapolated for mediator masses $M_{med} > 200\,GeV$. This is reasonable due to the smooth shape.

The following plots show the M_T shape in the **PS** model for different parameters. The additional ratio plot shows, that there is no difference (for different g_W) in the shapes besides the scaling. The ratio is calculated with the first drawn distribution and all other distributions. The labeling has the following form: [varied parameter,normalized]

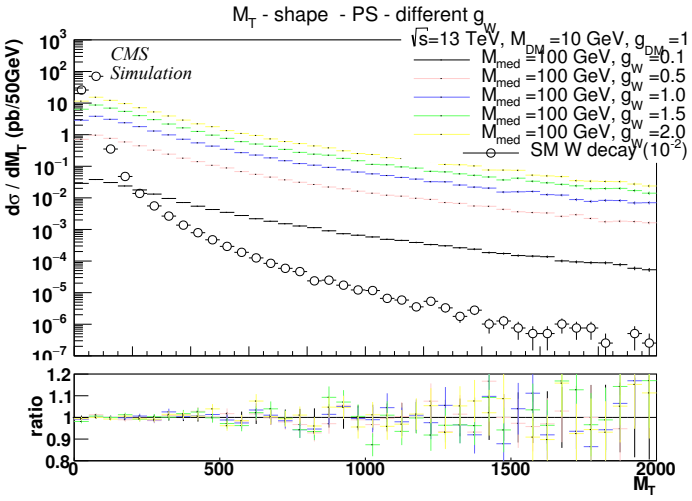

Figure 71: [g_W,not]

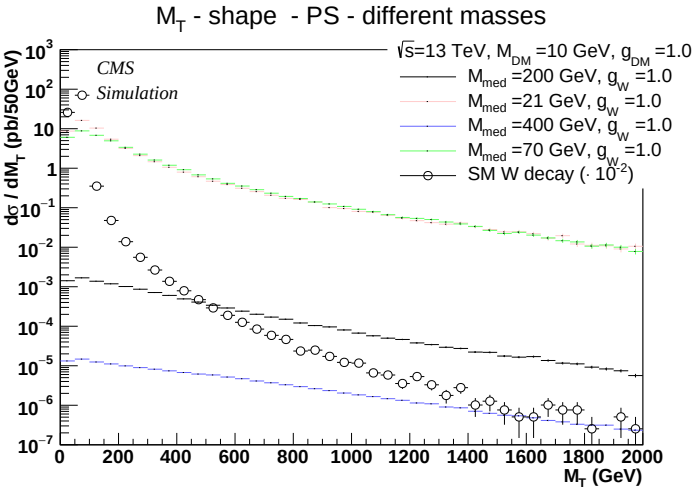

Figure 72: [M_{med},not]

The following plots show the η shape of the lepton in the **PS** model for different parameters. The appended ratio plots show the ratio of the distributions and the first drawn distribution (if the line at one is dotted) / the SM background (if the line is drawn through). The labeling has the following form: [varied parameter,normalized]

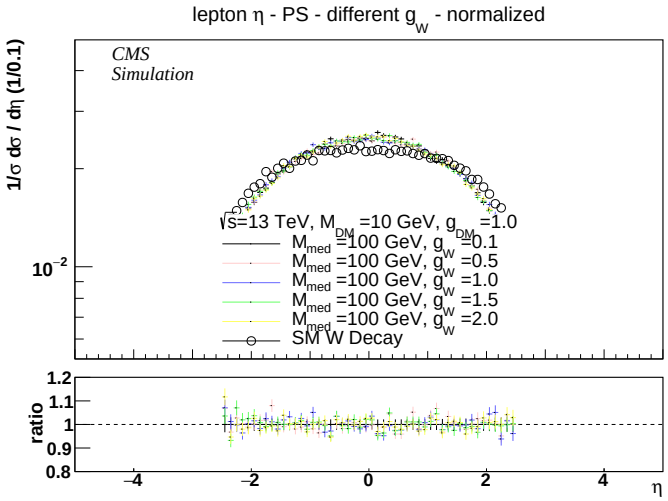

Figure 73: [g_W,yes]

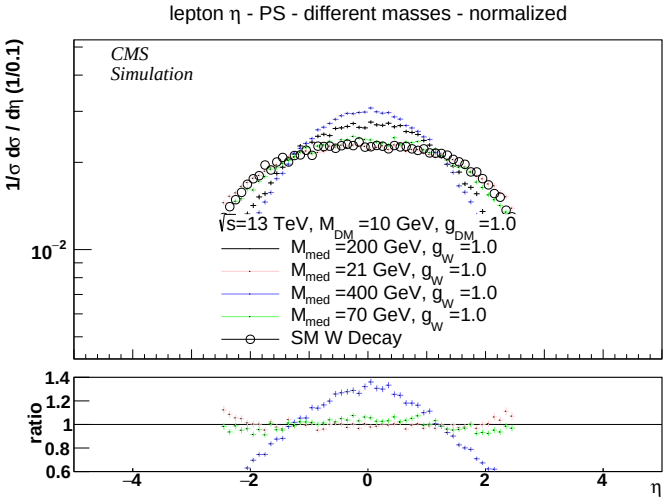

Figure 74: [M_{med},yes]

The following plots show the ϕ shape of the lepton ϕ_{lep} and the $\Delta\phi$(W,med) shape in the **PS** model for different parameters. The appended ratio plots show the ratio of the distributions and the first drawn distribution (if the line at one is dotted) / the SM background (if the line is drawn through). The labeling has the following form: [distribution,varied parameter,normalized]

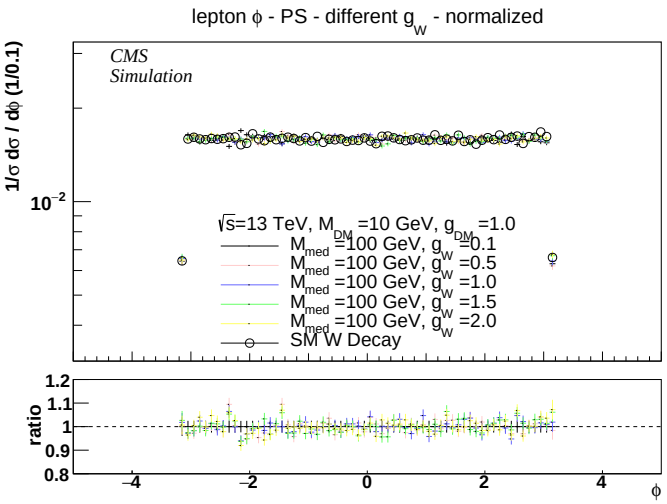

Figure 75: [ϕ_{lep},g_W,yes]

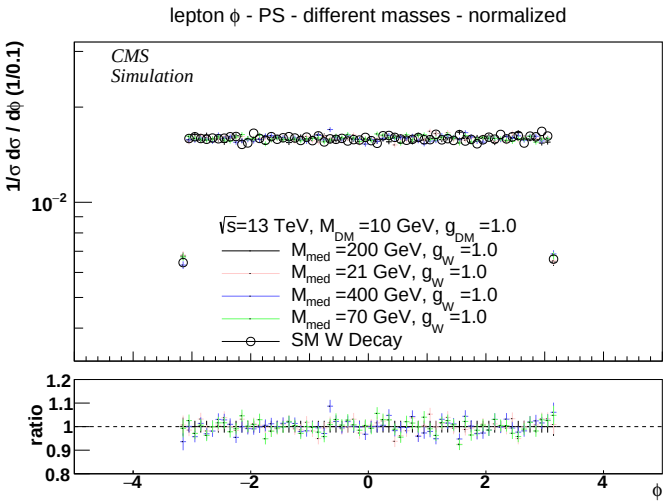

Figure 76: [ϕ_{lep},M_{med},yes]

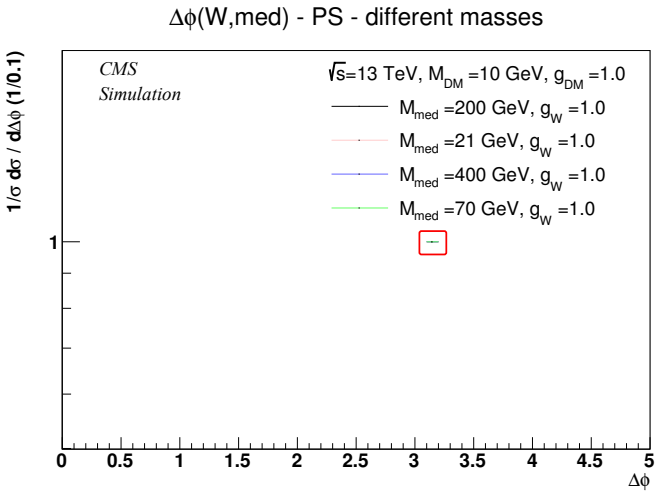

Figure 77: [$\Delta\phi$(W,med),M_{med},yes]

The following plots show the expected limits in the **PS** model. These are generated with a GEANT4 full simulation. The limits are produced for integrated luminosities of (1,30,300 and 3000) fb^{-1}. The labeling has the following form: [model]

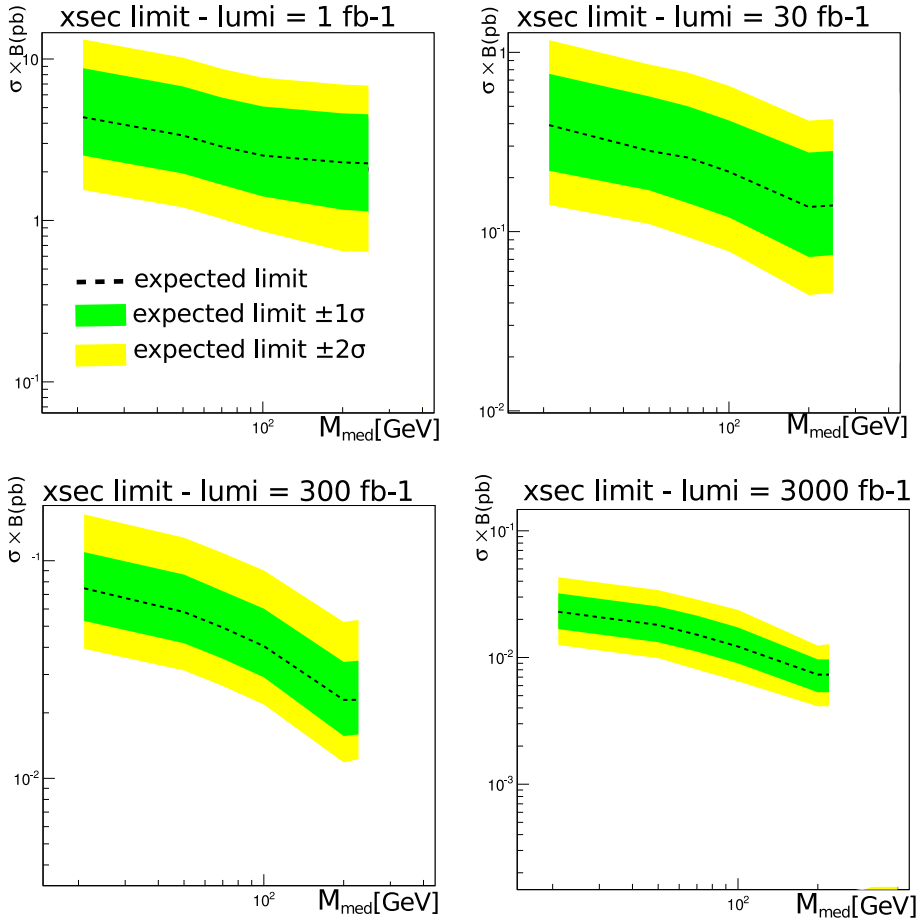

Figure 78: [PS]

6.3.2 Cross Section Analysis in the PS Model

The cross section scan of the pseudoscalar model is shown in Fig. 79. It is visible that the range, in which the cross section raises, is 10 orders ($10^{-7} - 10^{3}$ pb) in the used parameter boundaries. The cross section is very dependent on the chosen parameters. Especially a huge M_{med} dependence is found.

If the coupling strengths to the W Boson (g_W) has reached a certain point ($g_W \approx 0.3$), the cross sections dependent on the mediator mass exclusively.

The expected limits show, that for small mediator masses ($M_{med} < 200$ GeV), observations could be possible for even small luminosities ($< 30 fb^{-1}$). But to fully scan the mediator mass ($M_{med} > 250$ GeV) very high lumi is needed as well as in the S model. A discovery of a mediator mass of $M_{med} = 250$ GeV and higher is impossible even with a lot of data ($> 3000 fb^{-1}$).

The following plot shows the cross section dependence on two parameters. The parameters are varied in the two dimensional grids introduced in table 3. The dotted lines are the expected limits transferred from Fig. 78. Additionally the width exclusion criterion of $\Gamma_{\text{med}} \overset{!}{\leq} M_{\text{med}}/3$ is added to the plots.
The labeling has the following form:
[first varied parameter | second varied parameter,model,width approach]

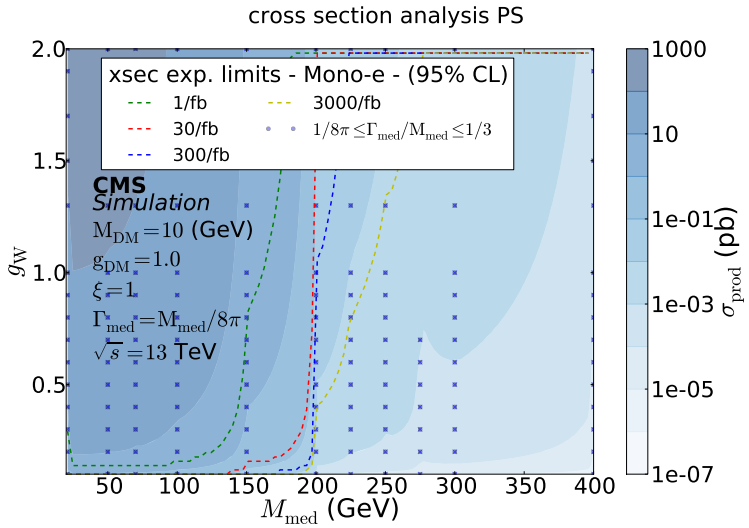

Figure 79: [M_{med} | g_W,PS,Γ_{nar}]

6.4 Model Comparison of the AV, S and PS Model

Now that every model has been discussed on its own, a comparison of the different coupling structures will follow.

A little complication in the model comparison emerges due to the computation difficulties for the PS and S event generation (see section 5.2). That is why one cannot compare all three models for all parameter sets. We will study the difference in the AV, S and PS model for smaller mediator and DM masses. The chosen parameter set is:

$$M_{\text{med}} = 100\,\text{GeV}; M_{\text{DM}} = 10\,\text{GeV}; g_{q/W} = 1.0\,; g_{\text{DM}} = 1.0$$

First we compare the shapes: We will take a look at the usual (yet studied) parameters like M_T and the η and ϕ distributions.

When comparing the M_T shapes of the different models (see Fig. 80), a big difference in cross section and shape is visible. Whereas the PS has the biggest cross section for this specific parameter set, it has the most outstanding shape as well. That the PS signal is the most easy to observe for this specific parameter set due to the best significance.

All three distributions shape in a low M_T region ($M_T < 200\,\text{GeV}$) in an different way than the $W \rightarrow l\nu$ background. Due to possible other backgrounds like fake electrons instead of a photon or Z→ll decays with an undetected lepton. A further look into other possible backgrounds is advised. Althought the shape looks different in the low M_T region, scanning this region is not possible because the background distribution is to high and so does not allow to see a significant number of signal events.

The M_T shapes vary within the three models (see Fig. 80). Thus it is a good tool to resolve the different coupling structures in further data analyses for this DM generation channel. The problem here is, that the mediator mass also varies the M_T shape into each model. Thus a direct

association M_T-shape $\leftrightarrow$model is not possible, but we must first resolve the mediator mass and can than analyse the M_T shape in respect to one of our 3 models. We can decide if the mediator couples S, PS or AV.

The same works the other way round. If we identified an AV,S or PS mediator, we can resolve the mediator mass with the M_T shape.

A significant fact is that the cross sections for S and PS couplings are highly dependent on the mediator mass M_{med}. This is not the case for the AV case (can be seen in Fig. 26).

This occurs due to the assumed branching ratios ($BR(\text{med} \rightarrow \text{DM}) = 1$) for the cross section analysis in the S and PS model.

When comparing the η shapes of the signals in Fig. 82 we find the same results as in the S and PS chapters. Scanning to the η shape has not been considered for DM search in our work group yet. A study of the η shape after a full simulation and with the detector efficiencies is advised.

As shown above, all three models rend ϕ independent distributions (see Fig. 83).

We did not look at the lepton p_T shape called p_T^{lep} till now. This is done in Fig. 81. This is the only real quantity that we can measure more or less immediately. What we can see here is the same attributes as for the M_T shape of the signals. The PS is the most outstanding case and all three models differ for this particular parameter case from the SM W background. Especially in a high p_T region, the PS is very outstanding to the other shapes.

This comparison has just been done for one parameter set. To fully resolve the differences between the models, a full scan and a full comparison for all parameter sets has to be done. After this scan, it will be possible to choose the most significant models in respect to the different parameters.

The AV model is the only model that is sensitive on high mediator masses ($M_{med} \gtrsim 200\,\text{GeV}$). The S and the PS model show no sensitivities for high mediator masses ($M_{med} \gtrsim 200\,\text{GeV}$). The difference in the cross sections in the S and the PS model can be explained by the parity violation in the electroweak interaction. Recently a paper [24] about the hadronic mono-jet channels showed, that there is almost no difference of the cross section from the S and PS case. In this model the mediator does not couple directly to the W boson but is produced in a top loop. In our model, the mediator and the W boson couple directly. This difference in the discussed channels hints that the extra spin sensitivity of the pseudoscalar mediator can answer this question. A study of the parities in the discussed channel shows that processes with a scalar mediator are highly suppressed. The coupling W$\leftrightarrow$med is weak. Thus the parity in this process is violated maximally. The formula for the parity of two particles is $P = P_1P_2 \cdot (-1)^L$ where L is the total angular momentum. This angular momentum is zero in this process in first order. The W boson has the parity P= -1 as well as the pseudoscalar particle. The scalar particle has the parity P= $+1$. Now we see that if the W radiates a scalar or pseudoscalar particle, the parity is only maximally violated for the pseudoscalar case. If the W radiates a scalar, the parity is conserved. This shows, that the scalar process is suppressed. That is the reason why the scalar cross sections differ so much from the pseudoscalar cross sections.

The following plots show various distributions to compare the three models (**AV**,**S** and **PS**). The appended ratio plots show the ratio of the distributions and the SM background. The labeling has the following form: [distribution,normalized]

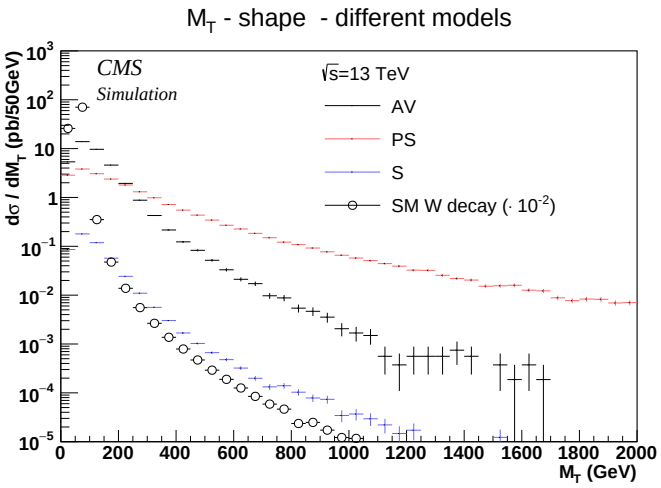

Figure 80: [M_T-shape,not]

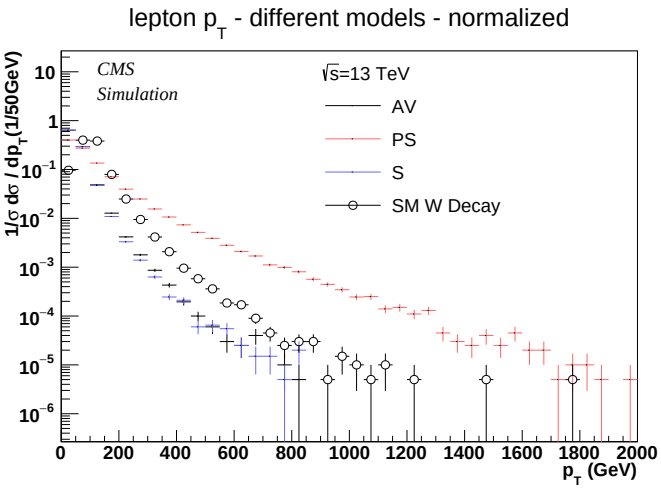

Figure 81: [p_T^{lep}-shape,yes]

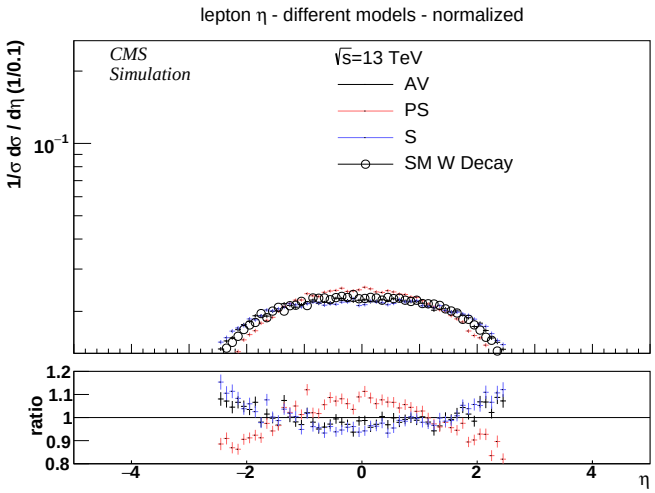

Figure 82: [η-shape,yes]

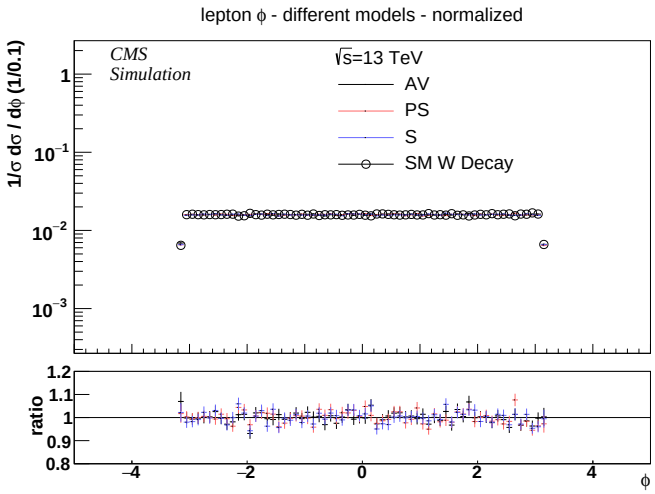

Figure 83: [ϕ-shape,yes]

6.5 The Background

The M_T spectrum and other shapes have always been discussed in comparison to a SM W decay background ($W \rightarrow e\nu_e$). This decay was generated with MG5. To keep the statistics up for the background distribution for high M_T we used two different distributions with 200000 entries each. These distributions are cutted at a total invariant lepton mass of $m_l^{tot} = 100\,\text{GeV}$, one time below, one time above this threshold. Subsequently the two distributions are assembled. This gives proper statistics for the low and high M_T regions.

This distributions peaks at the W mass at $M_T = 80.4\,\text{GeV}$.

The SM W provides a good comparison because the same W decay occurs in the discussed DM generation process.

So if we compare the difference of the two processes (background and DM production), the only difference is occurring because of the additional med-DM process.

If the difference between the background and the signal shape is big, a sufficient deviation between the expectation and the measurement, that would lead to a DM discovery, would be visible for comparative small luminosities. If the difference between the background and the signal is small, a lot of data must be collected to make a possible DM discovery.

7 Summary of the Observations

The coupling strengths vary the cross sections of a process in every coupling model but **do not** vary the signal shapes in any scanned signal for the analyzed models. They just scale the cross sections of the DM generation process in this simplified model. Therefore it is impossible to resolve the coupling strengths with the scanned shapes after a DM discovery. As mentioned we did not find a shape dependence from the coupling strength but we found a strong shape dependence from the coupling structure (AV,S or PS).

In this channel we find a high dependence of the observables and the underlying coupling model. The difference between the cross sections of scalar and pseudoscalar processes is big (for the same parameters: $\sigma_{\text{pseudoscalar}} \approx 100 \cdot \sigma_{\text{scalar}}$). This occurs due to the extra spin sensitivity from the pseudoscalar and is caused by the parity violation in the weak interaction (see section 6.4). Therefore the PS delivers better sensitivities in the scanned parameter space.

The cross section region that is covered by the AV model is included in the S and PS model. The last two cover a huge cross section region for the scanned parameters and show a high cross section dependence especially from the mediator mass M_{med}. We did not find this high mediator mass dependence in the AV model for a heavy mediator.

We observed in the AV model, that the DM mass does only barely change the event cross section. This is due to the fact that we initially demand a mediator with a defined width to decay into DM to 100%. This effect was expected.

The cross section analysis in the AV model is only dependent on the DM particle because M_{DM} and g_{DM} change the mediator width. This is more physical than the narrow width approach ($\Gamma_{\text{nar}} = M_{\text{med}}/8\pi$) in the S and PS model (see section 8).

We showed within this thesis, that the choice of the coupling model in respect to the mediator mass is very important in this channel. The scalar and the pseudoscalar model show no sensitivities for high mediator masses ($M_{\text{med}} \gtrsim 200\,\text{GeV}$). A search for DM with a heavy mediator can not be performed within an S or PS model. The model of choice to resolve heavy mediators ($M_{\text{med}} \gtrsim 200\,\text{GeV}$) is the AV model.

As shown in the AV model, the width of the mediator is very important for this study. A narrow width approach may not be directly motivated physically but produces the best significances in the light of new discoveries. A full scan of one model should always be done for at least two width approaches - the narrow width $\Gamma^{\text{nar}}_{\text{med}}$ that shows the best regions for a possible discovery and the largest width $\Gamma_{\text{med}} = M_{\text{med}}/3$. This way the two extreme cases of the width are discussed and show the criteria for a physically reasoned process and a possible DM discovery.

A scan of the M_{T} shape is the best method to search for DM in all three models. This M_{T} scan has been performed in our DM workgroup till now. This scan on the M_{T} shape should be made in the high M_{T} region, where the background is low.

A discovery in the low M_{T} region is highly suppressed due to a huge background.

8 Future Prospects

Subsequent to this thesis, some tasks and questions can be answered. We want to give a short overview about various topics, that might be approached following this thesis.

Till now the narrow width approach was chosen in the S and PS model. It would be good to see what happens in the S and PS model for different mediator widths. We recommend a search with the $\Gamma_{\text{med}} = \text{max.} = M_{\text{med}}/3$ approach as well to have simulated both outer boundaries of the mediator width. The other option is to implement the mediator width particle dependent, as done for the AV model. A mediator width that depends on the DM particle is physically well motivated. We implemented this feature in Madgraph for the AV model yet. This dependence should be implemented to the JHUGen event generation as well in the future.

Dependent on the mediator mass, the PS has an outstanding significance compare to the AV. Additionally a scan for the PS for run 1 data could be performed.

A full simulation in respect to the η shape of the signals could be done. This way it would be possible to compare how well possible deviations in the η shape can be seen in respect to the efficiency of the detector.

A good task for the future would be to implement the S and PS coupling in Madgraph via Feynrules [25]. Madgraph is a common and often used too in various CMS simulations. The problem with the JHUGen is that the usage is still quite raw and the documentation is incomplete. It may be a good tool for S and PS coupling mediators but was very hard to use. Even the DM generation is operable only because Phil Harris provided an extra tool for this. So in the future the JHUGen could be better understood, especially much more detailed - how it works and what it does.

References

[1] P. Harris, V. V. Khoze, M. Spannowsky, and C. Williams, "Constraining Dark Sectors at Colliders: Beyond the Effective Theory Approach," *Phys. Rev.*, vol. D91, no. 5, p. 055009, 2015.

[2] G. Bertone, *Particle dark matter observations, models and searches*. Cambridge, UK New York: Cambridge University Press, 2010.

[3] D. Fehling, "The Standard Model of Particle Physics." `https://upload.wikimedia.org/wikipedia/commons/0/00/Standard_Model_of_Elementary_Particles.svg`, 2008. [Online; accessed 17-July-2015].

[4] The CMS Collaboration, Khachatryan, Vardan *et al.*, "Search for dark matter, extra dimensions, and unparticles in monojet events in proton–proton collisions at $\sqrt{s} = 8$ TeV," *Eur. Phys. J.*, vol. C75, no. 5, p. 235, 2015.

[5] T. Saab, *An Introduction to Dark Matter Direct Detection Searches & Techniques*. 2013.

[6] K. I. of Particle Astrophysics and Cosmology, "Direct Dark Matter Detection." `http://kipac.stanford.edu/kipac/research/dark_matter_detection`. [Online; accessed 21-July-2015].

[7] J. Conrad, "Indirect Detection of WIMP Dark Matter: a compact review," in *Interplay between Particle and Astroparticle physics London, United Kingdom, August 18-22, 2014*, 2014.

[8] The CMS and ATLAS Collaborations, "Atlas + cms dark matter forum recommendations," *CMS + ATLAS*, 2015.

[9] The CMS Collaboration, Thomas,L. *et al.*, "The potential to study exotic physics signatures at hl-lhc using the phase 2 upgraded cms detector," *CMS*, 2015.

[10] The CMS Collaboration, Chatrchyan, S. *et al.*, "The CMS experiment at the CERN LHC," *JINST*, vol. 3, p. S08004, 2008.

[11] S. Erdweg, "Search for dark matter and w' in the final state with one muon and missing transverse energy with cms," 2013.

[12] L. Taylor, "CMS detector design." `http://cms.web.cern.ch/news/cms-detector-design`, 2011. [Online; accessed 17-July-2015].

[13] The TOTEM Collaboration, G. Antchev, *et al.*, "Luminosity-independent measurement of the proton-proton total cross section at $\sqrt{s} = 8$ TeV," *Phys. Rev. Lett.*, vol. 111, p. 012001, Jul 2013.

[14] The CMS Collaboration, V. Khachatryan, *et al.*, "Search for physics beyond the standard model in final states with a lepton and missing transverse energy in proton-proton collisions at $\sqrt{s} = 8$ TeV," *Phys. Rev. D*, vol. 91, p. 092005, May 2015.

[15] Y. Bai and T. M. P. Tait, "Searches with Mono-Leptons," *Phys. Lett.*, vol. B723, pp. 384–387, 2013.

[16] N. F. Bell, Y. Cai, J. B. Dent, R. K. Leane, and T. J. Weiler, "Dark matter at the LHC: EFTs and gauge invariance," 2015.

[17] O. Buchmueller, M. J. Dolan, S. A. Malik, and C. McCabe, "Characterising dark matter searches at colliders and direct detection experiments: Vector mediators," *JHEP*, vol. 01, p. 037, 2015.

[18] P. Schmüser, *Feynman-Graphen und Eichtheorien für Experimentalphysiker*. Springer, 1995.

[19] S. Agostinelli *et al.*, "GEANT4: A Simulation toolkit," *Nucl. Instrum. Meth.*, vol. A506, pp. 250–303, 2003.

[20] "Measurement of CMS Luminosity," Tech. Rep. CMS-PAS-EWK-10-004, The CMS Collaboration and CERN, 1900. Geneva, 1900.

[21] Phil Harris *et al.*, "Simplified models dark matter - dark matter signals using powheg and jhugen," *PCH SMS Update*, 2015.

[22] R. Brun and F. Rademakers, "ROOT: An object oriented data analysis framework," *Nucl. Instrum. Meth.*, vol. A389, pp. 81–86, 1997.

[23] R. M. Barnett *et al.*, "Review of particle physics. Particle Data Group," *Phys. Rev.*, vol. D54, pp. 1–720, 1996.

[24] T. C. Collaboration, "Search for new physics in the v-jet + met final state," *CMS PAS EXO*, 2015.

[25] N. D. Christensen and C. Duhr, "FeynRules - Feynman rules made easy," *Comput. Phys. Commun.*, vol. 180, pp. 1614–1641, 2009.

I want to thank the whole DM workgroup in the Institute of Experimental Particle Physics III A for the support and the fruitful discussions. Namely I would like to thank Dr. Kerstin Hoepfer, Klaas Padeken and Viktor Kutzner. Additionally I want to thank all the co workers at the Institute of Experimental Particle Physics III A for a very nice and comfortable working atmosphere. A large and additional thanks to the MuSiC people, for using the MuSiC machine.

9 Appendix

9.1 The W Polarisation in the Mono-e Channel

We showed an imbalance in the neutrino (and hence the electron as well[17]) movement concerning the W direction. We now ant to find out where this imbalance comes from.

We yet said that it is a polarization effect. To confirm this, we look at the electron movement concerning the W. First we analyse the different polarization states of a W boson. The following figure (Fig. 84) shows the dependence of the W boson polarization and the direction of the electron.

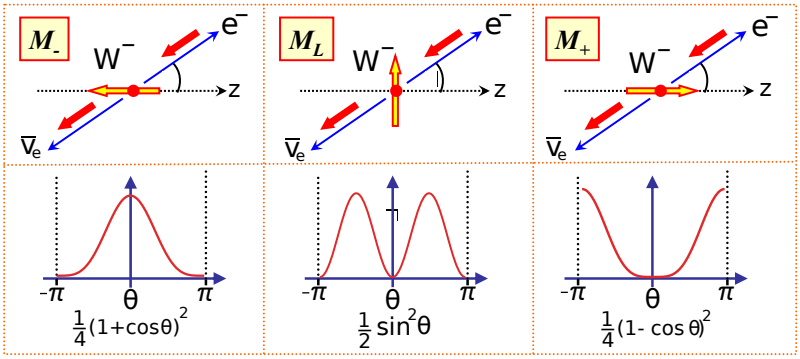

Figure 84: The dependence between the different W polarization and the kinematics of the electron.

We will do this in the rest frame of the W boson.

In the next plot (Fig. 85), we can see the $\Delta\Phi(\text{electron}, \text{W})$ plot for different mediator masses M_{med} and different interference cases (ξ).

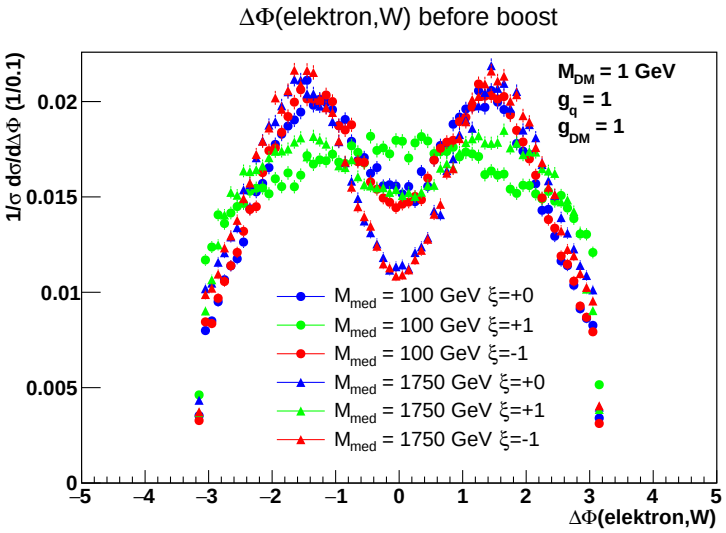

Figure 85: Different distributions of $\Delta\Phi$(electron,W) for different mediator masses M_{med} and the different interference parameters $\xi = \pm 1/0$.

Now we see that for light mediators in the discussed case ($\xi = +1$) we see the transverse

[17] In the rest frame of the W, the electron and the neutrino have to recoil totally due to the energy and momentum conservation.

polarized case (M_- - green cyrcles and triangles[18] in Fig. 85) prefered. Therefore the electron is more likely to go into the W direction. Hence the neutrino is more likely to go into the opposite direction as the W. This is what we found in the $\Delta\Phi(\text{neutrino}, \text{W})$ plot in the shape analysis of the AV model.

In the cases $\xi = +1/0$ longitudinally polarized W bosons are produced. This raises the cross sections into divergences. These divergences can just be normalized with a Higgs sector, as done in the SM.

Therefore studying these cases would reveal something about the Higgs sector of the DM particle. This is a complete new physical view and access to this particle in the case of a possible DM discovery.

We see as well that the question about the interference parameter ξ is not trivial and still not clarified. This question about the interference probably will be one of the most important questions in the DM search in the next years.

[18]The polarization in these cases has longitudinal parts but more M_- polarization than the other cases discussed in this figure.

Ich versichere, dass ich die Arbeit selbstständig verfasst und keine anderen als die angegebenen Quellen und Hilfsmittel benutzt sowie Zitate kenntlich gemacht habe.

Aachen, den